Universität Zürich[UZH]

Department of Geography

Soil Organic Carbon Dynamics in Mediterranean Landscapes: The Role of Pedogenesis, Land Use, and Glauconite in the Corleone Region, Sicily

GEO 511 Master's Thesis

Author: Annette den Boer, 19-731-694

Supervised by: Prof. Dr. Markus Egli, Prof. Salvatore Raimondi (salvatore.raimondi@unipa.it)

Faculty representative: Prof. Dr. Markus Egli

25.04.2025

Abstract

Soil organic carbon (SOC) is important for soil health and climate change mitigation through carbon sequestration. This study assesses the spatial distribution, composition, and stabilization mechanisms of SOC in the Corleone region of western Sicily, an area proposed for UNESCO Geopark status. Focus is placed on the influence of glauconite-rich Corleone Calcarenites on soil development and SOC dynamics. Nine soil profiles representing diverse land uses and soil types were analyzed for organic and inorganic carbon content. SOC was fractionated into particulate organic carbon (POC) and mineral-associated organic carbon (MOC) using density and aggregate-size fractionation. To analyze carbon sequestration mechanisms, oxalate extractable contents of Al and Fe, elemental composition and general soil characteristics (grain size, pH, C/N ratio, bulk density, soil skeleton content) were examined.

SOC stocks ranged from 6.24 kg C/m² in erosion-prone Cambisols to 24.7 kg C/m² in Vertisols and forested areas. While no significant differences were found between aggregate-size fractions, SOC content correlated positively with oxalate-extractable Fe ($R^2 = 0.32$, $p < 0.05$). Weathering degree showed a positive correlation with well-crystallized iron oxides and clay content, suggesting a more stable carbon pool in weathered soils. Profiles developed on Corleone Calcarenites exhibited higher SOC stocks in deeper horizons compared to those on Numidian Flysch, suggesting that glauconite supports SOC stabilization via mineral-organic complex formation and increased oxyhydroxide content.

Overall, the Corleone region demonstrates strong potential for long-term SOC sequestration. Sustainable land management practices are recommended to enhance this capacity and support climate resilience through improved soil carbon retention.

Acknowledgements

I would like to express my gratitude to my supervisor Markus Egli for his continuous support throughout this thesis. His guidance during fieldwork and willingness to answer my questions despite a busy schedule were invaluable. I also wish to thank Salvatore Raimondi for his role in organizing and facilitating the field campaign in Sicily, making this research possible. Despite some language barriers, I was able to learn a lot from him about the island and the soil properties in Corleone. Special thanks go to the lab technicians Yves Brügger and Barbara Siegfried whose expertise, patience and willingness to share their knowledge helped immensely during my lab work. I am also grateful to everyone who assisted in the field, especially those who helped dig the soil profiles, giving my muscles a small break.

I'd also like to thank my colleagues at Gruner for their understanding and flexibility, which allowed me to balance work and the writing of this thesis. Finally, I am deeply thankful for the support of my family, friends, and my partner, whose encouragement and understanding helped me through every stage of this journey.

Contents

List of Figures

List of Tables

List of Equations

1 Introduction

In 2019, the Rotary Club proposed to establish a Geopark in the Corleone region of Sicily. While Corleone, a town south of Palermo, is mostly known for its association with the Mafia, its history dates back to some of the earliest human settlements in the area (Raimondi & Pirrone, 2020). The region also has a unique geomorphological landscape due to its glauconitic calcarenite formations and significant palaeontological content, including fossils of fish teeth, oysters and large benthic foraminifers (Egli et al., 2021, 2024). Corleone's economy today depends primarily on agriculture, which affects local soil properties. The proposed Corleone Geopark aims to highlight the "Glauconitic Limestone of Corleone" as an area of geological, environmental, landscape, historical and cultural significance. However, the development of a Geopark has highlighted significant data gaps on soil characteristics, their genesis, their stability and erosion susceptibility in the region, particularly in terms of soil carbon data.

Soil organic carbon (SOC) is an important driver for ecosystem productivity, influencing soil microorganisms and soil structure. As a central element of soil organic matter it contributes to nutrient availability and soil fertility and is of essence to feed a growing world population (J. Gerke, 2022). Understanding the mechanisms that govern soil organic carbon storage and stability is crucial in the context of climate change mitigation, sustainable agriculture, and ecosystem health. In Mediterranean regions like Sicily, SOC dynamics are particularly complex due to the interplay of diverse soil types, variable land use practices, and distinct climatic conditions. The projected Corleone Geopark region offers a unique setting to investigate these dynamics, given its rich geological history, widespread agricultural activity, and presence of distinctive lithological units. This study aims to explore the factors influencing SOC variation, with a particular focus on soil type, land use, and the potential stabilizing effect of glauconitic calcarenite. By combining physical and chemical fractionation methods with site-specific analyses, this research seeks to enhance the understanding of SOC sequestration mechanisms in Mediterranean soils, contributing valuable insights to regional soil management strategies and broader environmental concerns.

1.1 Background information on soil organic carbon

Soils consists of different components, one of which is soil organic matter (SOM). It is a key component of soil, influencing fertility, nutrient cycling, and water retention (J. Gerke, 2022; Smith et al., 2015). It consists of living organisms, plant roots, and decayed material, which microorganisms break down into SOM. The composition of SOM varies depending on plant species, climate, and soil

type (Zollinger et al., 2013). SOM introduces carbon to the soil, some of which is stored as soil organic carbon (SOC) (Edwards, 2024). SOC stabilization is vital for climate change mitigation, as stable carbon pools reduce atmospheric CO_2 levels. The carbon cycle in the soil is complex and affected by different factors. Some of the carbon that enters the soil via plant biomass and is processed by microorganisms, binds to minerals or oxyhydrates, stabilizing it for extended periods (Wiesmeier et al., 2019).

SOC distribution varies globally, with colder, moist regions storing more carbon due to slower decomposition, while warmer, drier climates promote faster breakdown and lower SOC stocks (Jobbágy & Jackson, 2000; Wiesmeier et al., 2019). Peatlands illustrate this, accumulating large carbon stores due to limited microbial activity (Smith et al., 2015).

1.1.1 Fractions of SOM and SOC

SOM is commonly divided into two key fractions: particular organic matter (POM) that is easily accessible to microorganisms and thus subjected to fast decay and mineral associated organic matter (MAOM) protected from decay through intense interaction with mineral surfaces. These two fractions differ in their function, components, and residence times (Lavallee et al., 2020; Six, Conant, et al., 2002; Smith et al., 2015). POM is composed of lightweight fragments that are easily decomposed by microbes, resulting in short residence times (Lavallee et al., 2020). Its carbon component, Particulate Organic Carbon (POC), drives soil fertility but is vulnerable to land-use changes (Georgiou et al., 2022). MAOM on the other hand binds to mineral surfaces, protecting it from fast decomposition through the occlusion within small aggregates (Lavallee et al., 2020) and forms a stable carbon pool known as Mineral-Associated Organic Carbon (MOC). MOC decomposes slowly (over decades to centuries) and plays a crucial role in long-term carbon sequestration (Georgiou et al., 2022).

1.1.2 SOC fractionation techniques

This thesis aims to identify the different carbon fractions present in the studied soils. As previously described, soil carbon exists as particulate organic carbon (POC), mineral-associated organic carbon (MOC), and inorganic carbon, each with distinct stabilization mechanisms, turnover rates, and roles in soil fertility. Before fractionation, total carbon content is typically measured as a baseline for comparison (Laudicina et al., 2015; Martí-Roura et al., 2019; Viret & Grand, 2019). Then several fractionation methods are available. Chemical fractionation isolates specific soil components. Sodium hydroxide can extract organic components, while 10% H_2O_2 targets easily oxidizable organic matter, leaving behind resistant material (Zollinger et al., 2013). Acid hydrolysis quantifies older SOM, and alkaline extraction isolates mineral-bound SOM (Viret & Grand, 2019). Other techniques applied are radiocarbon dating to differentiate between old and young carbon pools, as well as stable isotope

analysis (Egli et al., 2007, 2021; Mastrolonardo et al., 2013; Zollinger et al., 2013). Biochemical Methods use microbial oxidation to study labile SOM but are often incomplete and destructive (Laudicina et al., 2015; Viret & Grand, 2019). Physical Fractionation is widely used and considered a reliable method (Viret & Grand, 2019). For this density fractionation can be used, which separates soil based on particle density, typically using liquids with densities between 1–1.85 g/cm³. The resulting light fraction (LF) contains young, undecomposed organic matter (POM/POC) with fast turnover, while the heavy fraction (HF) holds mineral-bound organic matter with slower decomposition rates (Mastrolonardo et al., 2013; Zollinger et al., 2013). Grain Size Fractionation separates soil into size classes (e.g., <63 µm for clay/silt and >63 µm for coarser particles). Clay-sized particles stabilize MAOM due to their larger surface area, while coarser particles are linked to fast-cycling POM/POC (Egli et al., 2007; Viret & Grand, 2019). Combining both techniques through Combined Size and Density Fractionation (CSDF) improves accuracy by better identifying organo-mineral associations (Viret & Grand, 2019). CSDF is effective across various soils and offers a practical approach for assessing carbon fractions, though pairing it with chemical analysis can enhance data quality, albeit with increased resource demands (Egli et al., 2007; Rovira et al., 1998; Zollinger et al., 2013).

1.1.3 Inorganic carbon

While organic carbon stocks are higher globally, inorganic carbon (IC) also plays a significant role in the carbon cycle. It is commonly found in arid and semi-arid soils, often in the form of carbonate minerals ($Ca/MgCO_3$), formed through reactions between bicarbonate and base cations or from carbonate-rich parent materials like limestone (Huang et al., 2024; Smith et al., 2015).

The global inorganic carbon pool is estimated at 750 Pg C to a depth of 1 m (Smith et al., 2015) and 2305 ± 636 Pg C to 2 m depth (Huang et al., 2024). Carbonate formation, influenced by water movement, nitrogen inputs, mineral composition, and pedogenesis, has been recognized as an effective carbon sequestration process (Naorem et al., 2022).

1.1.4 Carbon in the Mediterranean and Sicily

For the mediterranean region of Europe few studies have been conducted on quantifying SOC. Research focusing on Riparian forest ecosystems in the mediterranean find that SOC stocks are generally lower than those observed in temperate regions (Fernandes et al., 2020). With high temperatures in the mediterranean climate, organic matter inputs can be limited and decomposition is increased due to higher microbial activity, hindering accumulation of SOM and SOC (Edwards, 2024). In Mediterranean forests and rangelands, SOC content averages 60–70 t C/ha in the upper 30 cm, though values vary significantly (Rodeghiero et al., 2011).

In Sicily, SOC concentrations are influenced by altitude, with lower SOC levels at higher elevations (Egli et al., 2007). In the Etna region, precipitation and temperature also impact SOC — more rainfall reduces SOC, while warmer temperatures increase it (Egli et al., 2007). The Mediterranean climate's variability, combined with frequent disturbances like wildfires, further restricts SOC accumulation. Fire events, particularly in low-altitude areas, can increase labile biomass inputs, influencing SOC stocks (Mastrolonardo et al., 2013). A study in the Corleone region reported an average SOC content of 2.5%, with significant stabilization linked to the region's mineral composition (Egli et al., 2024). SOC accumulation rates are connected to weathering and were initially high in investigated transformed soils but declined over time (Egli et al., 2021).

1.1.4.1 SOC and land-use dynamics in the Mediterranean

Post-war agricultural reforms in Sicily have intensified cultivation, reducing SOC through conventional tillage and land conversion (Michelangeli et al., 2022; Quijano et al., 2017). Consequently SOC stocks were found to be consistently lower in agricultural soils than in forests or rangelands (Rodeghiero et al., 2011). However, land abandonment has shown potential for SOC recovery, reducing CO_2 emissions by ca. 887,745 Mg CO_2 in Sicily (Novara et al., 2017). Similarly, shrub clearing has been found to increase SOC stocks by 31.6% in Mediterranean soils (Cortijos-López et al., 2024).

Despite these insights, significant knowledge gaps remain regarding SOC inventories and carbon fraction dynamics in Sicily. Strategies such as cover cropping, minimal tillage, and agroforestry offer promising approaches to enhance SOC sequestration.

1.1.4.2 Inorganic carbon

In Mediterranean soils, inorganic carbon often dominates in arid and semi-arid areas, while SOC is more prevalent in wetter zones (Rodeghiero et al., 2011). Research by Egli et al. indicates that high carbonate contents are present in Sicilian soils (Egli et al., 2021, 2024). This corresponds to findings by Huang et al. (2024), who have investigated global inorganic carbon stocks, displaying them in a map of the world with Sicily showing comparably high stocks. In Corleone secondary carbonates form up to 50% of total inorganic carbon, implying active weathering processes in the region and an active cycling of organic and inorganic carbon (Egli et al., 2021). These secondary carbonates result from dynamic soil processes like leaching and reprecipitation.

High inorganic carbon stocks in Sicily align with global patterns identified by Huang et al. (2024), linked to the region's semi-arid climate and seasonal water availability. Secondary carbonates in Corleone's limestone-rich soils buffer pH, potentially influencing organic matter decomposition and nutrient cycling (Zhou et al., 2019).

1.2 Introduction to the study area

Sicily's diverse soils play a vital role in its traditional agricultural landscape, which covers about 63% of the region (Rodeghiero et al., 2011; Venturella, 2004). The most common soil types — Regosols, Lithosols, Cambisols, and Luvisols — contribute to variations in soil organic carbon and soil inorganic carbon storage. Key crops include grain, vine, olive, citrus, and orchards, with agroforestry also prominent in some areas (Barbera et al., 2012).

The study area lies in western Sicily near Palermo, specifically in the Corleone region. Samples were collected at elevations between 600 and 1000 m.a.s.l., with site details provided in chapter 2.1. Corleone's warm, temperate climate (average annual temperature of 15°C) and distinct wet-dry seasonal pattern (700 mm annual rainfall) (Climate Data, 2024) promote SOC cycling in winter and secondary carbonate formation in dry summers (Edwards, 2024). The region's bioclimate varies from the Lower Mesomediterranean zone (upper dry climate) to the Lower Supramediterranean zone (lower subhumid climate) (Bazan et al., 2015). The area shows a high level of biodiversity which is characterized by the presence of pasture and farming (Marino et al., 2017). The hilly landscape makes the area prone to erosion, influencing soil development. In Sicily, such topographical variation has contributed to diverse soil types, with mountainous regions often featuring young soils shaped by parent rock material and climate (Venturella, 2004).

Corleone's geological history is equally significant. The region lies within the Maghrebian-Sicilian fold-and-thrust belt, featuring Mesozoic carbonate deposits from shallow- and deep-water successions alongside Oligo-Miocene Numidian flysch formations (Basilone, 2011). Archaeological remains in Sicily date back over 20'000 years (Giannitrapani, 1998). These characteristics offer valuable insights into soil dynamics, agriculture, and carbon cycling — knowledge that may apply to other Mediterranean and semi-arid regions.

1.3 Corleone Calcarenite

Geological maps by ISPRA and Basilone (2011) highlight the Corleone Calcarenites, a distinct lithological unit. These formations consist of biocalcarenites and quartzose glauconitic sandstones with carbonate bioclasts, alternating with sandy marls containing planktonic foraminifera. The calcarenites, formed in a deltaic environment during transgressive-regressive cycles, vary in thickness from 10 to 80 meters(Instituto Superiore per la Protezione e la Ricerca Ambientale (ISPRA), 2024)

Calcarenite, a clastic limestone composed of calcitic or aragonitic particles (Orme, 1984), is geologically significant due to its mineral composition and depositional history. While the largest

outcrop of the formation is located in Corleone, smaller occurrences are present in other districts of the Belice, Eleuterio, and Milicia river basins (Raimondi & Pirrone, 2020). Corleone's Calcarenites are enriched in glauconite, a green, iron-rich clay mineral that forms in low-sedimentation marine environments (Hesse & Schacht, 2011; Tribovillard et al., 2023). Glauconite's slow formation over millions of years enhances soil fertility by releasing nutrients and promoting the development of kaolinite, ferruginous illite-smectite, and iron oxides during weathering (Egli et al., 2024). These processes are important for soil fertility and plant nutrients, showing the geological importance of this unit for agricultural activities in the region.

Historically, Corleone's Calcarenites have provided building materials and influenced settlement patterns (Raimondi & Pirrone, 2020). These formations also shape unique landscapes, such as the Two Fortresses Waterfall, which highlights the area's geological distinctiveness.

1.3.1 Carbon dynamics

The Corleone Calcarenites have not been thoroughly studied to date and there exists a knowledge gap on the influence of the material on soil development. Research suggests Corleone's Calcarenites influence soil carbon dynamics through glauconite weathering, which releases divalent iron and promotes organic matter stabilization (Egli et al., 2024). This process enhances SOC sequestration by forming mineral-organic complexes that reduce microbial decomposition rates (Egli et al., 2021, 2024).

Human activity has shaped the landscapes of the Corleone Calcarenites. Traditional low-intensity farming practices, such as grazing and olive cultivation, have likely contributed to SOC accumulation by increasing organic matter inputs and reducing soil disturbance. Conversely, intensive land use or poor management may accelerate erosion, depleting SOC stocks (Egli et al., 2021; H. H. Gerke et al., 2016; Raimondi & Pirrone, 2020).

Despite emerging evidence of calcarenite's role in SOC sequestration, further research is needed to explore its full influence on soil development and carbon storage.

1.4 Pedogenesis in Mediterranean Soils

Soil formation is a gradual process driven by climate, topography, organisms, and parent material, which collectively shape soil structure and composition over time. Mediterranean soils exhibit a complex interplay between natural weathering processes and human activity (Egli et al., 2024; Lin, 2011; Raimondi & Pirrone, 2020).

Pedogenic processes such as mineral transformation contribute to soil development, while non-pedogenic processes like groundwater movement create distinct soil features (Jiménez-Ballesta et al., 2023; Phillips, 2017). Historical land use practices, including deforestation, grazing, and early irrigation, have influenced erosion rates and SOC accumulation patterns (Quijano et al., 2017).

In Mediterranean soils, carbonate weathering plays a crucial role, contributing to the formation of secondary carbonates that support soil development (Egli et al., 2021, 2024; Jiménez-Ballesta et al., 2023; Raimondi & Pirrone, 2020). While volcanic soils in the region have been studied in detail, Corleone's Calcarenites remain underexplored. Initial research indicates glauconite weathering in these soils enhances the presence of kaolinite, iron oxides, and other minerals that stabilize SOC (Egli et al., 2024).

1.4.1 Effect of pedogenesis and soil mass redistribution on SOC

Pedogenesis directly impacts SOC storage by stabilizing organic matter through clay mineral formation and soil aggregation. Organic carbon typically accumulates in upper soil horizons but can redistribute due to erosion and land management practices (Egli et al., 2021).

On slopes, erosion reduces SOC at eroded sites while depositing carbon-rich material downslope, creating varied SOC distribution patterns (H. H. Gerke et al., 2016). Research highlights that eroded soils, especially those on crests or exposed areas, are often shallow with reduced SOC content, while stable sites with optimal clay and oxyhydroxide compositions provide better SOC sequestration conditions (Egli et al., 2021). In Mediterranean systems, land management practices such as tillage and residue handling have a strong influence on soil redistribution, SOC storage, and overall pedogenesis (Quijano et al., 2017).

1.4.2 Climate variability and outlook

Mediterranean soils have developed over millennia in response to changing climates. With ongoing climate change, SOC dynamics are expected to shift, influencing the global carbon cycle (Albaladejo et al., 2013). Especially the upper soil horizons are expected to be affected by climate change as shown in models (Herzog et al., 2019; Lozano-García et al., 2017).

Increased temperatures and drought conditions can reduce vegetation cover, litter inputs, and SOC accumulation (Albaladejo et al., 2013; Rey et al., 2005) (Rey et al., 2005). Conversely, SOC may increase at deeper soil levels (Lozano-García et al., 2017). Studies show that summer droughts and sudden rain events accelerate carbon mineralization, further influencing SOC stability in Mediterranean regions (Rey et al., 2005).

1.5 Research questions

This study aims to investigate the factors influencing soil organic carbon dynamics in the projected Corleone Geopark region, focusing on variations across soil types, land use impacts, and the role of glauconitic calcarenite. The aim is to reduce some of the knowledge gaps previously mentioned and gain a deeper understanding of the region. Specifically, the research addresses three key questions:

1. How do organic carbon stocks vary across different soil types within the Corleone Geopark region?
2. What is the relationship between land use (e.g., agriculture, natural landscapes) and SOC content and composition in the Corleone region?
3. How does the presence of glauconitic calcarenite influence SOC sequestration and stability in Corleone soils?

Given the current understanding of soil processes in the Mediterranean and Corleone regions, several hypotheses have been formed:

- Agricultural soils are expected to contain lower SOC levels and altered carbon fractions compared to less-disturbed or natural soils. This reflects the impacts of tillage, erosion, and reduced organic matter inputs typically associated with intensive land use.
- Soils influenced by glauconitic calcarenite are hypothesized to exhibit enhanced SOC stability and sequestration potential. This is attributed to glauconite's contribution to soil structure, nutrient release, and the formation of mineral-organic complexes that protect organic matter from decomposition.

By addressing these questions, the study seeks to expand the understanding of soil carbon dynamics in Mediterranean landscapes, with potential insights applicable to similar environments affected by climate variability and land management practices.

2 Methods

The methodology was designed to answer the research questions presented in chapter 1.5. The methods include field sampling, laboratory analyses and statistical assessment to explore the interactions between soil properties, organic carbon dynamics, and environmental factors. The chosen methods are based on existing literature, leaning on research done in the region by Egli et al. (2021, 2024). This chapter is divided into several sections. Firstly, the study area is described, followed by the sampling strategy and detailed information on the sampling locations. Next, laboratory analyses are presented, followed by the statistical techniques used to process and interpret the data. By creating transparency showing the applied methodology, this chapter aims to support the validity of the research.

2.1 Study Area and sampling strategy

In chapter 1.2 background information about the study area has been introduced. The sample sites were chosen to represent the area of the proposed UNESCO Geopark with the help of an expert to the region, Salvatore Raimondi from the University of Palermo. Figure 4 shows the geological maps of the region with the different sampling sites indicated. Of the nine sample sites all but three (Nr. 1, 2, and 10) were taken of soil that has formed on Corleone Calcarenite. This unique parent material not only forms the foundation for the establishment of the Geopark but also contains the characteristic glauconites that influence both soil properties and carbon dynamics. The choice of sampling sites allows for the exploration of how soils derived from Corleone Calcarenite differ in pedogenesis compared to those formed on other substrates. The high glauconite content, rich in iron and clay-like minerals, contributes to distinct weathering processes and the potential for stabilization of soil organic carbon through interactions with mineral surfaces. The sites also reflect the geomorphological and land-use variability within the region. Different land-use types are included in the dataset: agricultural soils, soils used for grazing, forest soils, relatively untouched soils. The choice of these sites contributes to insights into how environmental factors and human activity impact SOC dynamics and pedogenic processes. By sampling across these diverse locations, the relationship between the unique geological substrate, soil development, SOC fractions, and land use is addressed, which is crucial for understanding both the scientific and ecological value of the proposed Geopark. The area is representative of a mediterranean climate, allowing for comparisons across existing datasets and literature.

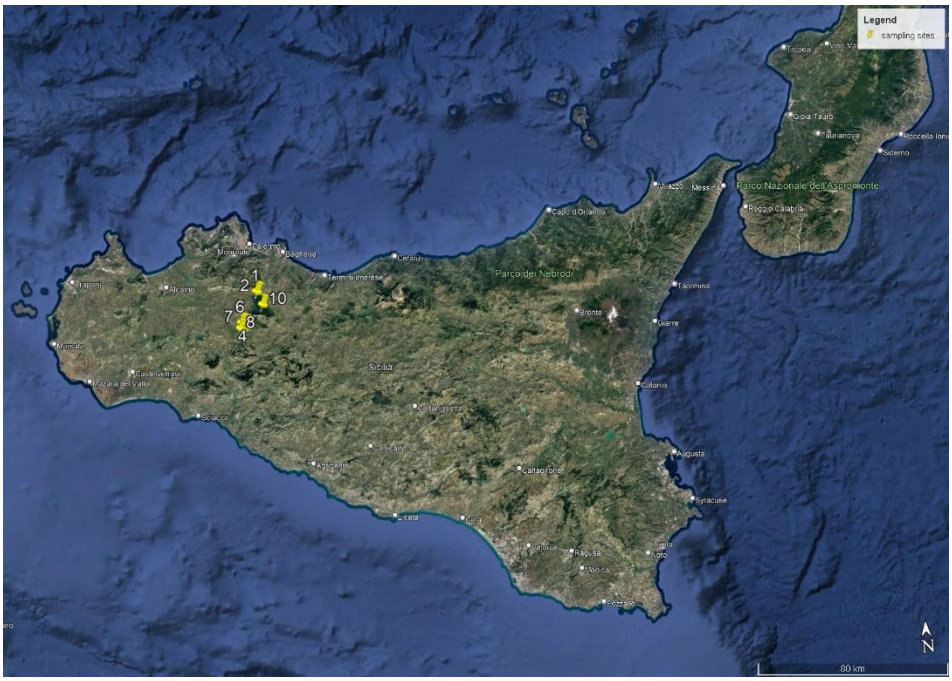

Figure 1: Orthofoto of Sicily, yellow pins indicating the sampling sites. Map data by Google Earth (2024).

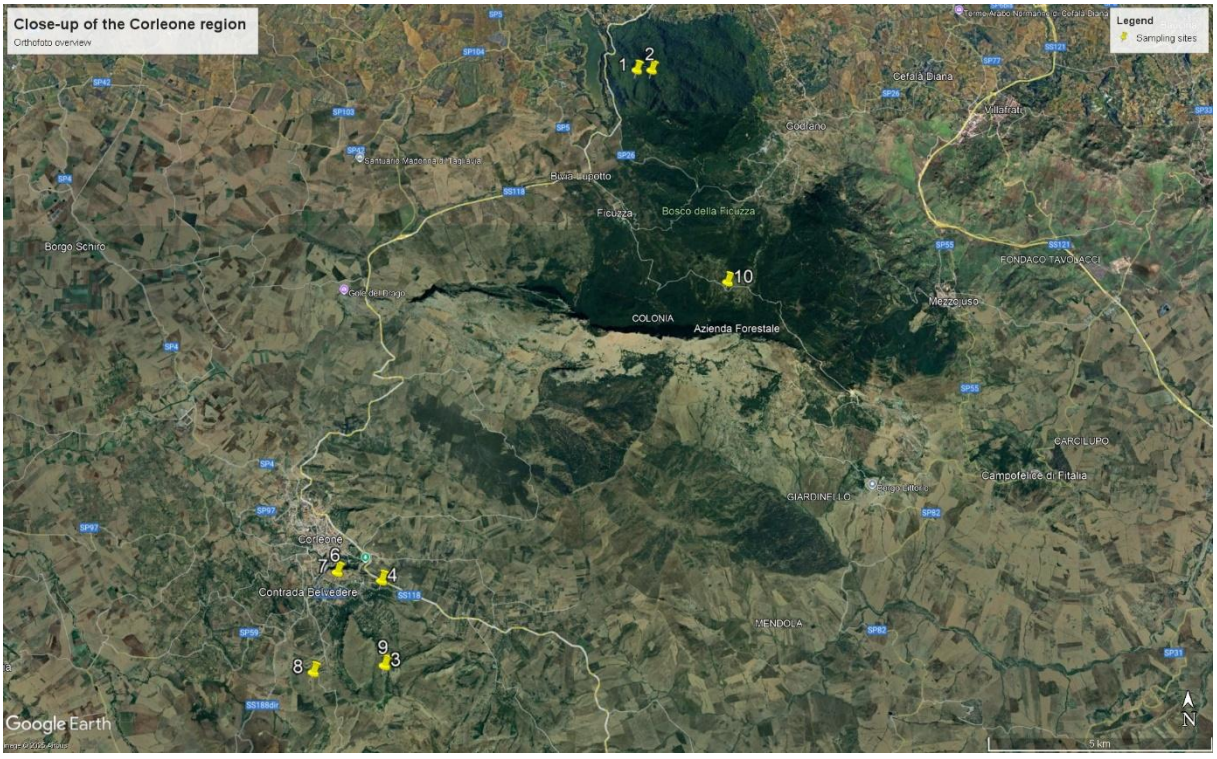

Figure 2: Close up of the Corleone region and the sampling sites marked in yellow. Map data by Google Earth (2024).

2.1.1 Sampling method

In total nine soil profiles were sampled in the first week of April 2024. The profiles were dug down to the C or R horizon, ensuring complete vertical stratigraphy. With the profiles ready, the different horizons were identified and described according to a sampling sheet. For determining the bulk density, two samples per horizon were taken using soil cylinders (100 cm^3, Eijkelkamp NL), including

both fine earth and coarse fragments. Additionally, all horizons of a soil profile were sampled with 0.7 – 1 kg of soil material using a simple shovel.

Profile 1

Profile 1 is located in Bosco della Ficuzza, a nature reserve for the protection of woods and wildlife (Regione Siciliana, 2024). The main land use form is agroforestry, with cows roaming around the forested hills. The forest mostly consists of evergreen and deciduous oak forests (Regione Siciliana, 2024). The profile was dug on a midslope facing eastward at 595 m.a.s.l. The soil type is Cambisol with some gleyic properties found in the lower horizon.

Profile 2

The second profile is located in the same nature reserve as profile 1, further up the hill at 650 m.a.s.l. The soil is more deeply developed and can be classified as Luvisol. The location has been undisturbed, which is shown by the mature soil and strong soil development.

Profile 3 and 9

The profiles 3 and 9 are both located on Montagna Vecchia, south of Corleone, which is a protected archaeological area. The plateau is of high archaeological interest as it was inhabited in prehistoric times and again in the Middle Ages (Spatafora, 1996). The mountain reaches its highest point at 1080 m.a.s.l. and the dominant vegetation is shrubs and grassland. The land is used as pasture, mainly for horses. The soil on the plateau is not deeply developed with only one Ah horizon present at both profiles and is classified as a Leptic Chernic Phaeozem.

Profile 4

Profile 4 is found in a deciduous forest close to Corleone at 705 m.a.s.l. The profile was dug on a midslope (15°) facing NW. The Vertisol has developed on the lithological unit of the Corleone Calcarenites (Instituto Superiore per la Protezione e la Ricerca Ambientale (ISPRA), 2024).

Profile 6 and 7

The two profiles were dug close to each other on a hill slope facing west. The area is used as grassland and pasture for horses and sheep. Even though the profiles lie close to each other, the different locations on the hills influence soil redistribution and the depth of the profiles. Profile 7, which is located at 662 m.a.s.l. has been more strongly eroded and shows a higher skeleton volume, resulting in a shallower soil profile. Profile 6 on the other hand at 658 m.a.s.l. seems to have accumulated some of this eroded material, resulting in a deeper soil profile. Both soils are Cambisols,

which are at the early stage of pedogenesis due to the disturbances at the site. The soils have both developed on Corleone Calcarenite as parent material.

Profile 8

At an elevation of 815 m.a.s.l. in a small valley used as agricultural grassland profile 8 was dug. The soil type is Vertisol with the profile showing a distinct reddish color.

Profile 10

Profile 10 is located in Bosco della Ficuzza just like profiles 1 and 2. Yet it is further to the North, close to the Rocca Busambra, a plateau towering over the national reserve. The profile was dug at 963 m.a.s.l. on a midslope facing NE. The Vertic Cambisol is a mature soil, which shows a deep profile.

2.2 Physical Analysis

In the laboratory different methods were used to assess the soil characteristics and specific components related to soil formation and SOC fractions.

2.2.1 Sample preparation

In the UZH labs all the samples were first dried at 40°C for 48 hours. We measured the moist and dry weights, to later calculate the moisture content of the soils from the volumetric samples. After drying, the soil samples were sieved with a 2 mm sieve to determine the coarse fragments. For further analysis only the bulk samples were used with the volumetric samples only relevant for the moisture content and calculation of soil density. This resulted in 24 samples. From each of these ca. 10 g of soil material was milled to < 50 µm.

The Bulk density was measured using the formula

$$\rho = \frac{M}{V}$$

Equation 1: calculation of soil bulk density

with V = 100 cm^3 and M=soil weight after drying.

2.2.2 Grain size analysis

Grain size is a key soil characteristic influencing carbon dynamics, as different grain sizes correspond to distinct carbon fractions. For grain size analysis, 50–55 g of fine soil was treated with 800 ml of 3% hydrogen peroxide (H_2O_2) to break down organic matter and separate grains, with heating used to accelerate the reaction. The prepared samples were sieved using a tower of eight sieves (32–2000

µm), which was sealed, connected to a water supply, and shaken until the outflow was clear. Sieves were then rinsed, and their contents transferred to ceramic bowls, dried overnight, and weighed to determine grain size distribution. Finer fractions (<32 µm) were measured using an X-ray SediGraph 5100 (Buurman et al., 1996). Before analysis, the device was calibrated with a baseline solution (20 ml of 0.5% sodium hexametaphosphate and 20 ml tap water). A 20–40 ml soil/water dispersion (3–5 g solids) was mixed with a 0.5% sodium hexametaphosphate solution (1:1), then homogenized via ultrasound (Bandelin Sonoplus HD 2070) for 5 minutes at 70% power (five cycles). The solution was transferred to the SediGraph mixing chamber, and measurement started immediately.

2.2.3 POM fractionation

To compare soil and carbon fractions, particulate organic matter (POM) was separated from the remaining soil material. For this, 10 g of fine earth was mixed with 100 ml of tap water, stirred, and left to settle for 24 hours. The mixture was then centrifuged at 5000 rpm for 10 minutes, and the supernatant containing solids (POM with a density <1 g/cm³) was discarded. Both fractions were dried at 40°C. The fraction with a density <1 g/cm³ yielded very little material and could not be used for further analysis. The >1 g/cm³ fraction was sieved through a 63 µm mesh, yielding two fractions associated with different carbon pools (Bonar et al., 2023; Martí-Roura et al., 2019). As dry sieving does not disrupt aggregates like wet sieving, the resulting fractions represent aggregate rather than grain size fractions. Total carbon, nitrogen, and isotope values were measured using TCD and EA, while LOI analysis determined organic carbon and carbonate content.

2.2.4 Total elemental content (XRF)

X-ray fluorescence (XRF) analyzes major and trace elements in geological materials by exposing atoms to X-rays, displacing inner electrons, and creating instability (Brouwer, 2010). An outer electron replaces the displaced one, releasing fluorescent radiation, which is measured to identify the elements present.

For measurement, plastic cups with thin foil were filled three-quarters full with fine-milled sample material and then sealed.

2.3 Chemical analysis

2.3.1 Soil pH

The hydrogen ion concentration is defined as the negative base-10 logarithm of the molar concentration of dissolved hydronium ions (H_3O^+), which indicates the acidity of the soil solution.

Measuring pH provides insight into the basic chemical state of the soil, affecting the decomposition of organic matter. In this analysis, the pH was determined using a 0.01 M $CaCl_2$ solution at a solid-liquid ratio of 1:2.5, using 5.0 g of soil (Pansu & Gautheyrou, 2006a). The mixture was then soaked, stirred, and left to rest. Finally, the combined glass electrode was placed into the suspension to measure the pH value.

2.3.2 Oxalate and Dithionite extraction

Dithionite extraction quantifies crystalline and non-crystalline pedogenic oxyhydroxides (Fe, Al), while oxalate extraction targets poorly-crystalline phases of the elements. The elemental concentrations in these solutions provide insights into the chemical composition and mineralogical properties of the samples, aiding in the identification of specific mineral fractions (Borggaard, 1988; Kaiser & Zech, 1996).

Oxalate Extraction: The oxalate solution is prepared by dissolving 16.1 g ammonium oxalate ($(NH_4)_2C_2O_4 \cdot * H_2O$, 0.11 mol) and 10.9 g oxalic acid dihydrate ($H_2C_2O_4 \cdot * 2H_2O$, 0.087 mol) in 900 ml of deionized water and adjusting the pH to 3. To perform the extraction, 2 g of soil was weighed, mixed with 100 ml of oxalate solution, and shaken in the dark at ~150 rpm for 2 hours. The suspension was then filtered using a 150 mm folded filter paper into a plastic bottle, separating the dissolved minerals from the soil particles.

Dithionite Extraction: 1 g of soil was weighed, and 8 ml of 0.3 mol/l sodium citrate solution (88 g $C_6H_5O_7Na_3 \cdot * 2H_2O$/l) and 2 ml of 1 mol/l sodium bicarbonate solution (84.0 g $NaHCO_3$/l) were added. The sample was heated in a water bath at 75–80°C, followed by the addition of sodium dithionite ($Na_2S_2O_4$). After reducing the temperature to 85°C, the sample was heated for another 15 minutes, then centrifuged until the solution was clear. The supernatant was transferred to a 100 ml volumetric flask. This process was repeated for consistency. The sample was then rinsed with 0.1 mol/l magnesium sulfate solution (24.6 g $MgSO_4 \cdot * 7H_2O$/l), centrifuged again, and the clear solution was added to the volumetric flask. Finally, the flask was filled to the 100 ml mark with deionized water. The same procedure was applied to blank and calibration solutions for standardization.

Elemental concentrations in both extraction solutions were measured using atomic absorption spectroscopy (AAnalyst 700, Perkin Elmer).

2.3.3 Loss on Ignition (LOI)

This method quantifies the organic content of a soil sample by burning the organic matter at high temperatures in the presence of oxygen. The resulting weight loss corresponds to the organic fraction, while the remaining residue represents the inorganic material (Pansu & Gautheyrou, 2006b).

For analysis, ca. 2 g of air-dried soil is placed in a crucible and heated at 550°C for 6 hours (Pansu & Gautheyrou, 2006b). After cooling in a desiccator, the crucible is weighed to calculate the loss on ignition (LOI) using the formula:

$$LOI = m1 - m2$$

Equation 2: Calculation of Loss on Ignition

where m1 is the sample weight before ignition and m2 after ignition.

2.3.4 Contents of total carbon and total nitrogen and isotope values

To assess the carbon inventory, total carbon (C) and nitrogen (N) contents were measured using a Thermal Conductivity Detector (TCD), which converts solids into gases, allowing for CO_2 and N_2 quantification. The analysis was performed with a Thermo Fisher Scientific Flash HT Plus elemental analyzer, equipped with a TCD and coupled to a ConFlo IV–Delta V Plus isotope ratio mass spectrometer. This provided $\delta^{13}C$ and $\delta^{15}N$ isotopic values, calibrated against in-house standards, including Chernozem and a laboratory caffeine standard. Isotopic values were referenced to Vienna Pee Dee Belemnite (V-PDB) for carbon and Atmospheric Nitrogen (AIR) for nitrogen.

2.3.5 Organic / inorganic carbon and carbonate content

During LOI, organic carbon is burned off, leaving only inorganic carbon in the sample. The inorganic carbon content can be derived from LOI values and elemental analysis results. For bulk samples and soil fractions >1 g/cm³, >63 µm, and >1 g/cm³, <63 µm, it was calculated as follows:

$$(1 - mass\ loss\ by\ LOI) \times total\ carbon\ content\ after\ burning$$

Equation 3: step 1 for calculation of organic carbon content

This value was then subtracted from the total carbon content of the untreated sample to determine the organic carbon content. The carbonate content was calculated using:

$$\frac{100}{12} \times inorganic\ carbon\ content$$

Equation 4: calculation of carbon content where 12 is the molar mass of C and 100 the molar mass of Ca in carbonate minerals

The results are presented in Table 4.

2.3.6 Chemical weathering indices

XRF analysis provides an overview of the elemental composition of soil samples. Major elements such as Ca, Mg, and Na naturally occur as oxides; therefore, their concentrations were first converted into their respective oxide forms. These percentages, along with loss on ignition (LOI) values, were

summed. Most samples had a total composition close to 100%, though some ranged from 93% to 111%. To ensure consistency, the data was normalized to 100%. From these results, various weathering indices (based on molar ratios) were calculated based on the comparison between a chemically stable mineral or compound and one that is more susceptible to weathering-induced depletion.

(Ca+K)/Ti: Since Ca and K are typically found in silicate minerals that break down during weathering, while Ti remains relatively stable, lower values indicate stronger weathering. Including total Ca also accounts for carbonate dissolution.

(Na+K)/Ti: This ratio is similar to (Ca+K)/Ti but reflects weathering of silicates.

Chemical Index of Alteration (CIA): The index is normally used for siliceous soils or igneous rocks. It reflects the accumulation of Al, with higher values indicating more intense silicate weathering (Nesbitt & Young, 1982). The formula used for the index is the following:

$$CIA = \frac{Al_2O_3}{Al_2O_3 + CaO + Na_2O + K_2O} * 100$$

Equation 5: Chemical Index of Alteration

Weathering index of Parker (WIP): This index is calculated using the following formula (Parker, 1970):

$$WIP = 100 * \left(\frac{2Na_2O}{0.35} + \frac{MgO}{0.9} + \frac{2K_2O}{0.25} + \frac{CaO}{0.7}\right)$$

Equation 6: Weathering Index of Parker

A lower WIP value suggests a higher degree of weathering.

Primitive mantle: Trace elements from the Earth's upper mantle can be used to analyze soil samples, with the composition of the primitive mantle provided by Sun and McDonough (1989). The ratio to the primitive mantle is calculated as follows:

$$\frac{element\ measured\ \left[\frac{mg}{kg}\right]}{element\ in\ primitive\ mantle\ \left[\frac{mg}{kg}\right]}$$

Equation 7: Ratio of trace elements to the primitive mantle

A high ratio indicates an enrichment of the measured element, while a low ratio suggests depletion compared to the primitive mantle.

2.4 Data analysis

For data collection and aggregation Microsoft Excel was used. For correlation analysis the Add-In for Microsoft excel "Analysis ToolPak" was used to calculate linear regression and R^2. Excel was also used for the creation of graphs and plots. Additionally, R Studio 2023.06.0 was used to analyze correlations. First a Shapiro-Wilkinson test was performed followed by a Spearman's rank correlation for not normally distributed data. For the analysis of distinction between the two groups (Numidian Flysch, Corleone Calcarenite), the Wilcoxon rank-sum test was applied, p – value= 0.05.

In Microsoft Excel different calculations were performed. Most have been mentioned in the previous paragraphs: Equation 1: calculation of soil bulk density, Equation 2: Calculation of Loss on Ignition, Equation 3: step 1 for calculation of organic carbon content, Equation 4: calculation of carbon content where 12 is the molar mass of C and 100 the molar mass of Ca in carbonate minerals, Equation 5: Chemical Index of Alteration, Equation 6: Weathering Index of Parker, Equation 7: Ratio of trace elements to the primitive mantle.

Additionally, the organic carbon stock per horizon was calculated as follows:

$$stock = thickness \times bulk\ density \times organic\ carbon\ concentration \times (1 - coarse\ fragments) \times 10$$

Equation 8: calculation of organic carbon stocks [kg/m²]

3 Results

Table 1: Overview and description of the sampled sites

Profile	Soil type, WRB	Coordinates	Altitude (m.a.s.l.)	Mean annual temp. (°C)	Annual precipitation (mm)	Slope (%)	Aspect	Slope position	Current land use
1	Eutric Cambisol	37°54'51''N 13°22'53''S	595	14-15	800	20	E	midslope	Agro-forestry
2	Nudiargic Luvisol	37°54'51''N 13°23'8''S	650	14-15	800	5	SW	midslope	pasture
3	Leptic chernic Phaeozem (protokalaic)	37°47'11''N 13°18'57''S	983	14-15	800	10	N	upper slope	Pasture
4	Haplic Vertisol	37°48'12''N 13°18'52''S	706	14-15	800	15	NW	midslope	Open deciduous forest
6	Calcaric Cambisol	37°48'18''N 13°18'10''S	659	14-15	800	11	W	midslope	Pasture
7	Calcaric Cambisol	37°48'18''N 13°18'11''S	661	14-15	800	18	W	midslope	Pasture
8	Pellic Vertisol	37°47'6''N 13°17'52''S	814	14-15	800	0		valley	Grassland
9	Leptic chernic Phaeozem (protokalaic)	37°47'11''N 13°18'57''S	995	14-15	800	10	N	upper slope	Pasture
10	Vertic Cambisol	37°51'58''N 13°24'20''S	963	14-15	800	11	NE	midslope	pasture

3.1 Physical and chemical soil characteristics

At the ten sampling sites, four different soil groups were identified according to the WRB (IUSS Working Group WRB, 2022). All the profiles have undergone human influences either many thousand years ago (for profiles 3 and 9) or by more recent usage as grassland or arable land. The depth of the soil profiles varied greatly with the shallowest profiles with only an Ah horizon (ca. 25 cm) found on la Montagna Vecchia (profiles 3 and 9) at a higher altitude and upper slope position. The profiles 2 and

10 in Bosco della Ficuzza show the most deeply developed soils, both profiles reaching a depth of approximately 120 cm. Most profiles exhibit a soil horizon sequence of A-B-C.

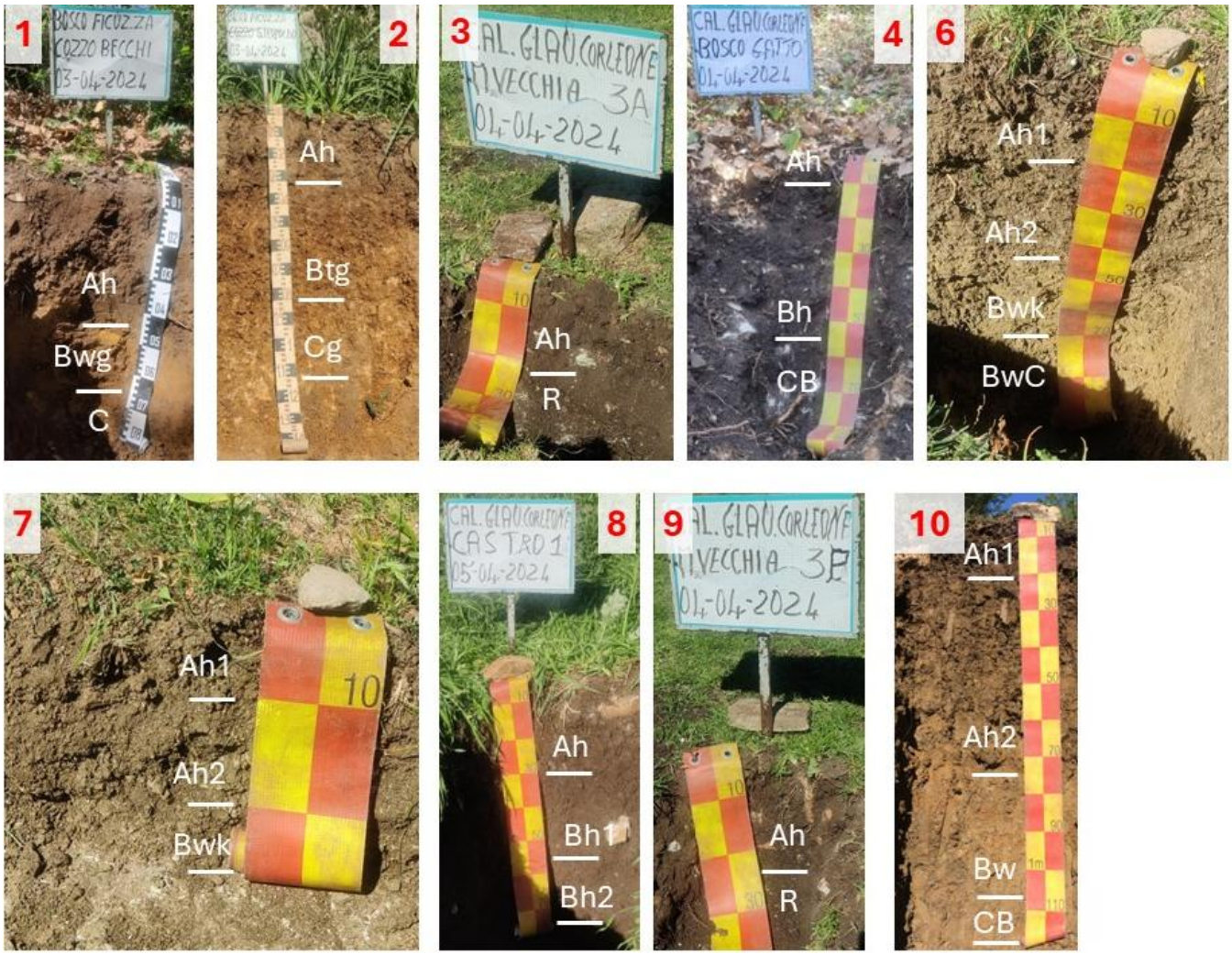

Figure 3: Soil profile photos with horizon designations of the sites 1-4 and 6-10

Grain size

The soils analyzed generally show high sand content, ranging from 22.6% to 60.9%, accompanied in some cases by substantial amounts of clay (24.8%–54.9%) (see Table 2). Silt consistently represents the smallest fraction across all profiles, with values between 8.8% and 28.7%. Profile 10 exhibits the lowest sand content (29.8%–43.1%) among all profiles and is characterized by higher clay levels. In contrast, Profiles 3 and 9, located on Montagna Vecchia, have the highest sand contents (60.9% and 56.4%, respectively), while still containing notable amounts of clay (25.6% and 32.6%). In most soil profiles, sand content is greatest in the upper horizon. Notably, clay tends to peak in the B-horizons, indicating accumulation processes. While silt is generally less dominant, Profiles 6 and 7—located close to each other—exhibit comparatively higher silt content, ranging from 12.1% to 28.7%.

Soil density and coarse fragments

The bulk density of the samples varies from 0.87 to 1.57 g/cm^3 with no identifiable trends across horizons or locations. Similarly, the skeletal content (>2 mm) varies greatly, with the locations 6 and 7 exhibiting the highest proportion of coarse fragments.

pH value

Carbonate content varies across profiles and is generally low, except in Profiles 6 and 7, where values range from 30% to 40%, peaking in the B-horizon (see Table 2). Consequently, the soils at these sites are slightly alkaline, with pH values between 7.4 and 7.7. Across the entire dataset, pH values span a broader range, from strongly acidic (pH 3.96 in Profile 2, horizon Btg) to slightly alkaline (pH 7.7 in Profile 7, horizon Bwk). Most soils fall within the neutral to slightly alkaline range (pH 6.0–6.8). Profile 1 exhibits slightly acidic conditions, while Profile 2—one of the deeper profiles—displays the most pronounced acidity. Interestingly, both these profiles developed on the same parent material, the Numidian Flysch (ISPRA, 2024). Profile 10, which shares this parent material, shows pH values more comparable to those of profiles developed on Corleone Calcarenite.

Parent material

Figure 4 presents the geological map of the study area, with the sampling locations marked. Profiles 1, 2, and 10 were taken from soils developed on Numidian Flysch, while Profiles 3, 4, 6, 7, 8, and 9 are derived from Corleone Calcarenite.

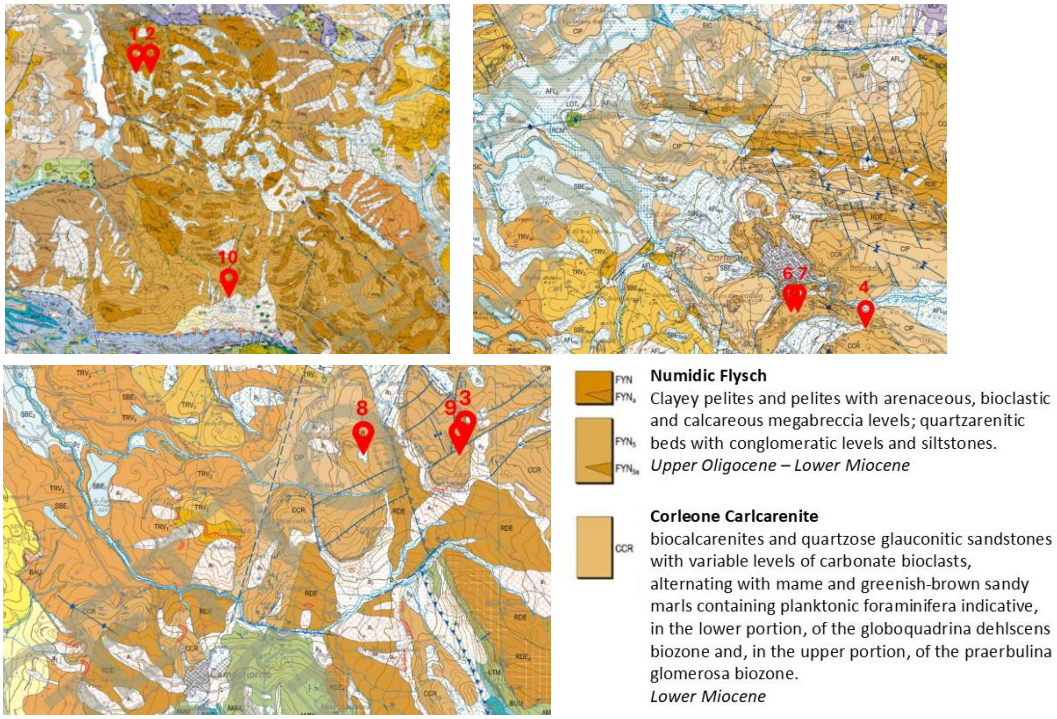

Figure 4: Excerpts from the geological maps of Sicily (Istituto Superiore per la Protezione e la Ricerca Ambientale) with the sampling sites indicated in red. (Legend entry translated from Italian using deepl.com)

Table 2: General soil characteristics

Site	Horizon	Depth	Soil type	Parent material (geological map)	Munsell moist	Coarse fragments	Bulk density	Sand	Silt	Clan	$CaCO_3$	pH	LOI
		cm				wt-%	g/cm^3	%	%	%	%	$CaCl_2$	%
Profile 1	Ah	0-45	Eutric Cambisol	Numidian Flysch	10YR 2/2	2.1	1.37	53.8	13.1	32.1	0.30	5.62	7.6
	Bwg	45-70	Eutric Cambisol	Numidian Flysch	10YR 6/8	1.9	1.57	43.2	11.7	44.1	0.43	5.02	6.5
Profile 2	Ah	0-40	Nudiargic Luvisol	Numidian Flysch	7.5YR 3/2	4.9	1.36	56.2	12.3	28	0.14	4.62	5.4
	Btg	40-80	Nudiargic Luvisol	Numidian Flysch	7.5Yr 4/6	2.3	1.09	34.1	13.9	51.2	0.42	4.05	7.7
	Cg	80-120	Nudiargic Luvisol	Numidian Flysch	10YR 7/4	1.1	1.29	56.2	13.1	29.9	0.25	3.69	6.7
Profile 3	Ah	0-20	Leptic chernic Phaeozem	Corleone Calcarenite	10YR 2/1	0.5	1.13	60.9	12.9	25.6	1.00	6.21	14.6
Profile 4	Ah	0-10	Haplic Vertisol	Corleone Calcarenite	7.5YR 3/2	6.4	0.87	52.6	13.1	33.5	1.15	6.54	19.5
	Bh	10-55	Haplic Vertisol	Corleone Calcarenite	7.5YR 3/2	1.0	1.09	52	11.1	36.3	0.92	6.51	11.3
	CB	55-80	Haplic Vertisol	Corleone Calcarenite	7.5YR 2/2	1.7	0.97	53.9	8.8	36.9	1.70	6.6	11.3
Profile 6	Ah 1	0-20	Calcaric Cambisol	Corleone Calcarenite	10YR 3/2	1.4	1.16	49.2	16	28.8	34.54	7.42	10.3
	Ah 2	20-45	Calcaric Cambisol	Corleone Calcarenite	2.5Y 4/3	28.7	1.44	47.8	21.1	27.9	38.23	7.39	8.9
	Bwk	45-70	Calcaric Cambisol	Corleone Calcarenite	10YR 5/3	8.6	1.39	36.1	28.7	33.8	39.05	7.41	9.2
	BwC	70-100	Calcaric Cambisol	Corleone Calcarenite	2.5Y 5/3	2.6	1.32	38.8	25.8	34.6	33.73	7.56	9
Profile 7	Ah 1	0-10	Calcaric Cambisol	Corleone Calcarenite	2.5Y 3/2	0.0	1.36	49.2	13.4	29.1	31.95	7.61	10.3
	Ah 2	10-20	Calcaric Cambisol	Corleone Calcarenite	2.5Y 4/2	2.5	1.1	52.4	12.1	28.6	30.82	7.54	8.6
	Bwk	20-25	Calcaric Cambisol	Corleone Calcarenite	2.5Y 4/3	13.0	1.19	51.9	18	24.8	39.90	7.7	7.8
Profile 8	Ap	0-30	Pellic Vertisol	Corleone Calcarenite	10YR 2/2	15.3	1.07	51.2	9.8	38.8	0.29	6.8	10.4
	Bh 1	30-55	Pellic Vertisol	Corleone Calcarenite	10YR 3/2	0.2	0.93	50.5	9.4	39.9	0.26	6.64	9.8
	Bh 2	55-75	Pellic Vertisol	Corleone Calcarenite	10YR 2/1	0.3	1.28	49.9	9.2	40.7	0.24	6.61	10.1
Profile 9	Ah	0-25	Leptic chernic Phaeozem	Corleone Calcarenite	10YR 2/1	0.4	1.01	56.4	9.6	32.6	3.76	6.81	15.7
Profile 10	Ah 1	0-20	Vertic Cambisol	Numidian Flysch	10YR 3/4	8.1	1.19	43.1	14.8	41.5	0.15	6.5	11.3
	Ah 2	20-75	Vertic Cambisol	Numidian Flysch	10YR 3/3	0.9	1.41	29.8	14.9	54.9	0.56	6.8	8.9
	Bwg	75-105	Verticke Cambisol	Numidian Flysch	10YR 4/3	2.3	1.27	34.0	15.4	49.4	0.18	6.78	8.8
	CB	105-120	Vertic Cambisol	Numidian Flysch	10YR 6/2	2.8	1.31	30.2	15.3	53.5	0.16	6.8	10.5

3.2 Pedogenic oxyhydroxides

Table 3 shows various aluminum and iron ratios, highlighting the distribution of crystalline and non-crystalline pedogenic oxyhydroxides extracted using dithionite (Al(d) and Fe(d)). These values vary across profiles, particularly for iron. Profile 8 displays the highest concentrations of both Al(d) and Fe(d), with relatively little variation across its horizons. In contrast, Profile 2 shows a nearly linear increase in Fe(d) with depth, accompanied by a rise in Al(d) within the B-horizon. A similar trend is observed for Fe(d) in Profile 10, which increases with depth but drops off in the CB-horizon (105–120 cm). Profiles 6 and 7 exhibit the lowest levels of Al(d) and Fe(d). No consistent depth-related trends can be observed in the remaining profiles. The ratio of pedogenic iron to total iron (Fe(d)/Fe(t)) is highest in the three profiles developed on Numidian Flysch (ranging from 0.48 to 0.57), as shown in Figure 7. In contrast, profiles formed on Corleone Calcarenite exhibit lower ratios (0.20–0.23), with Profile 8 standing out as an exception, showing elevated values (0.35–0.39).

Poorly crystalline forms of Fe and Al, extracted with oxalate, show a different pattern than the dithionite-extractable fractions. Profiles 1 and 3 exhibit the highest oxalate-extractable iron (Fe(o)) values in their upper horizons.

Crystalline Fe oxyhydroxides, calculated as the difference between Fe(d) and Fe(o), range from 0.5% to 3% and dominate over poorly crystalline forms in all profiles. The lowest crystalline Fe content is observed in the Ah horizon of Profile 3, while the highest is found in the Bw horizon of Profile 10. Profiles 2, 8, and 10 generally show high crystalline Fe contents (>2%), except for the Ah horizon in Profile 2 (0.8%). The proportion of total Fe present as crystalline oxyhydroxides is expressed by the ratio (Fe(d)–Fe(o))/Fe(t) (see Figure 7). This ratio varies widely across the dataset, from a minimum of 8% in the Ah horizon of Profile 3 to a maximum of 54% in the Cg horizon of Profile 2. Profiles 2 and 10 consistently show high values, with more than 40% of total Fe occurring in crystalline form in all horizons, indicating advanced weathering. Profile 1 also exhibits relatively high ratios compared to other sites. Notably, these three profiles are all derived from Numidian Flysch, distinguishing them from those formed on Corleone Calcarenite.

A Wilcoxon rank-sum test confirms a statistically significant difference in the (Fe(d)–Fe(o))/Fe(t) ratio between the two parent materials Corleone Calcarenite (median = 0.17) and Numidian Flysch (median = 0.44) ($W = 2$, $p = 6.119e{-}06$). A weaker but still significant difference is observed for the aluminum ratio (Al(d)–Al(o))/Al(t) ($W = 34$, $p < 0.05$).

3.2.1 Correlation of organic carbon with Al and Fe

The organic carbon stocks of the bulk soil were compared with the different iron fractions to explore potential relationships. While most comparisons revealed no significant correlations, a slight positive association was observed between Fe(o) and organic carbon stock (see Figure 5).

To check the data for normality, a Shapiro-Wilkinson test was applied to the data range. The results indicated that the crystalline form of aluminum (Al(d)–Al(o)) follows a normal distribution (p = 0.51), whereas the crystalline iron fraction (Fe(d)–Fe(o)) does not (p = 0.001). Organic carbon content in the soil was also found to deviate significantly from normality (p = 0.007). Consequently, non-parametric Spearman's rank correlation was applied to evaluate relationships between pedogenic oxide fractions and organic carbon.

A statistically significant negative correlation was found between the crystalline aluminum fraction (Al(d)–Al(o)) and organic carbon content (rs = –0.65, p = 0.001). For iron, however, no significant correlation emerged (rs = –0.35, p = 0.09).

3.2.2 Correlation of clay content with Al and Fe

No significant trends or correlations were observed between clay content and aluminum fractions. However, a clear relationship emerges between iron content and clay content. As illustrated in Figure 6, dithionite-extractable iron Fe(d) increases with rising clay content (linear regression: y = 639.47x – 4168.4, R^2 = 0.379, p = 0.001). A similar trend is observed for the crystalline iron fraction Fe(d) – Fe(o), which also shows a significant positive correlation with clay content (linear regression: y = 635.98x – 7631.6, R^2 = 0.427, p = 0.0005).

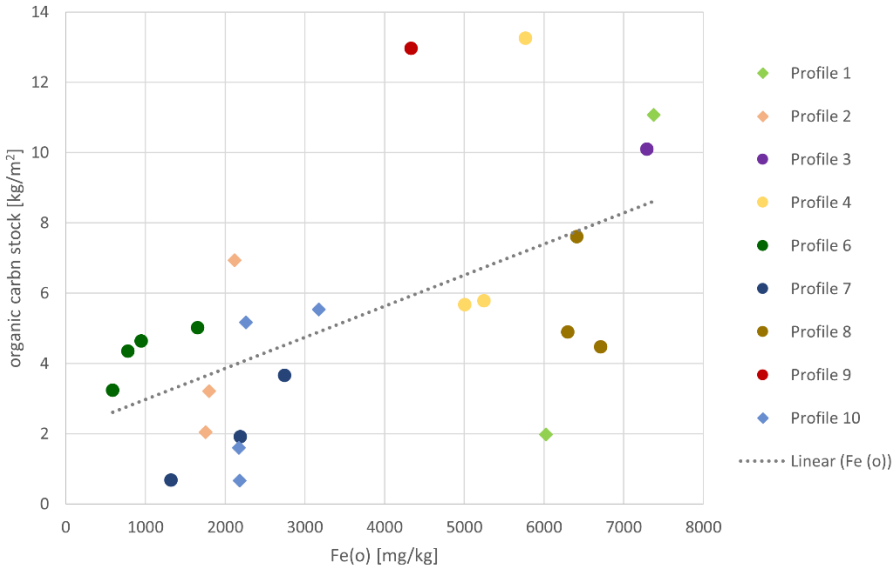

Figure 5: Linear regression of organic carbon stock and Fe(o). (y=0.0009x + 2.0838, R2 = 0.323, p-value = 0.0038)

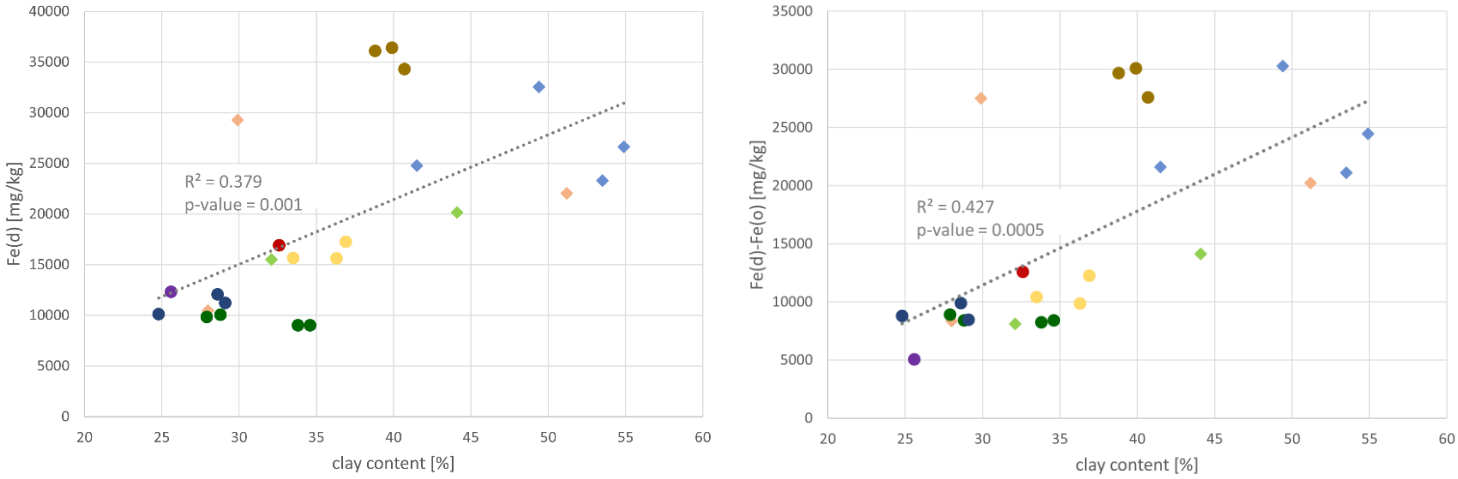

Figure 6: linear regression of clay content and Fe(d) and Fe(d)-Fe(o)

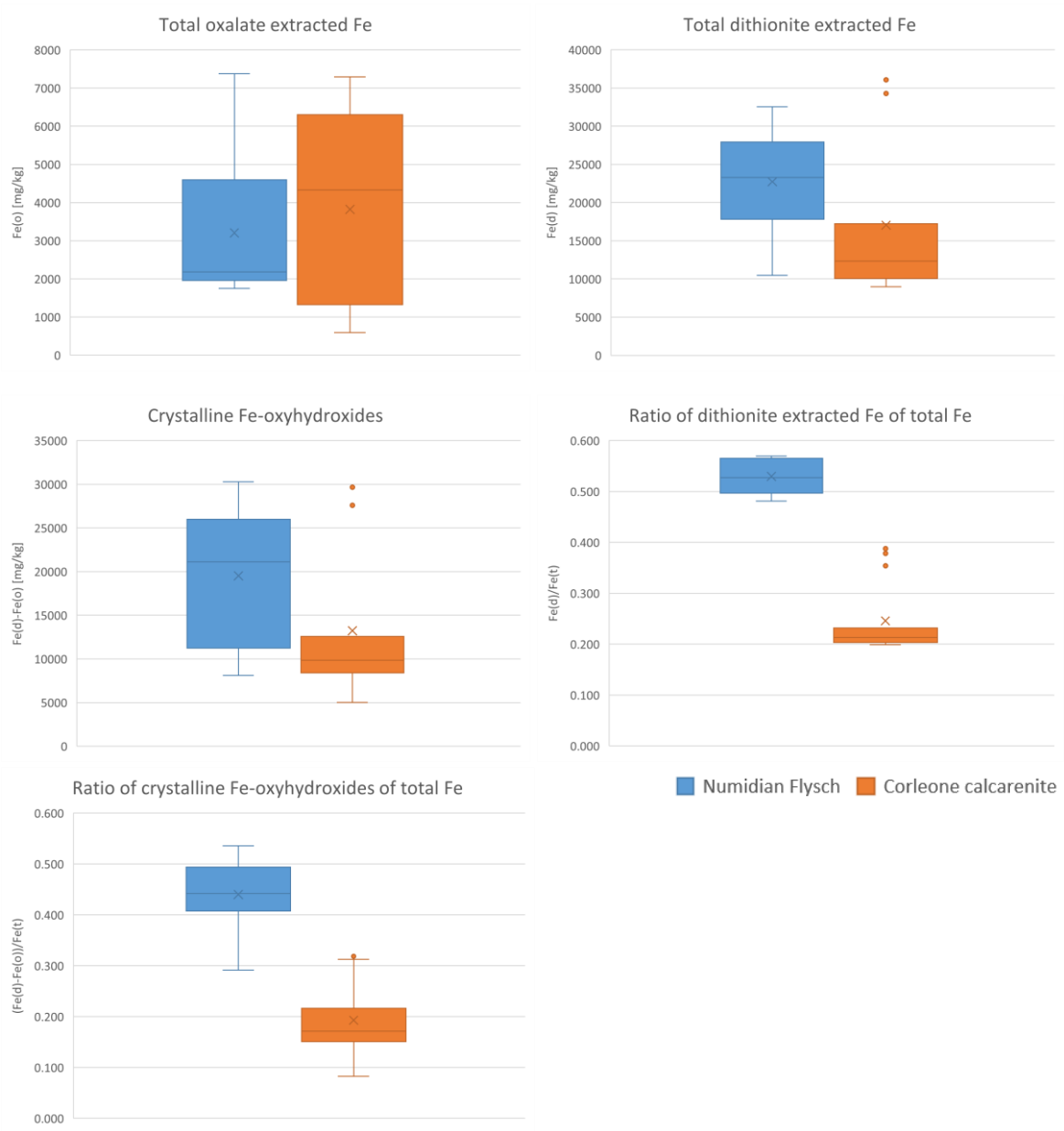

Figure 7: different forms and ratios of iron, comparing the two types of parent material: Numidian Flysch and Corleone Calcarenites

Table 3:Oxalate (o) and dithionite (d) extractable of Fe and Al. In addition, the well crystallised forms of Fe and Al were calculated and related to total content.

Location	Horizon	Parent material	Al (o) mg/kg	Fe (o) mg/kg	Al (d) mg/kg	Fe (d) mg/kg	Al(t) %	Fe(t) %	Al(d)-Al(o) mg/kg	Fe(d)-Fe(o) mg/kg	Al(o)/Al(t)	Fe(o)/Fe(t)	Al(d)/Al(t)	Fe(d)/Fe(t)	(Al(d)-Al(o))/Al(t)	(Fe(d)-Fe(o))/Fe(t)
Profile 1	Ah	Numidian Flysch	859	7374	946	15485	6.34	2.78	87	8111	0.014	0.265	0.015	0.556	0.0014	0.291
	Bwg		848.5	6024.5	1190	20135	8.81	3.57	341	14110.5	0.010	0.169	0.014	0.564	0.0039	0.395
Profile 2	Ah	Numidian Flysch	1095	2120	1422	10465	4.69	1.99	327	8345	0.023	0.107	0.030	0.527	0.0070	0.420
	Btg		2478.5	1800.5	3330	22025	9.48	4.58	852	20224.5	0.026	0.039	0.035	0.481	0.0090	0.442
	Cg		2837	1752	3138	29260	9.73	5.13	301	27508	0.029	0.034	0.032	0.570	0.0031	0.536
Profile 3	Ah	Corleone Calcarenite	2527.5	7292	1675	12330	4.81	6.07	-853	5038	0.053	0.120	0.035	0.203	-0.0177	0.083
Profile 4	Ah	Corleone Calcarenite	2224	5246.5	1361	15660	5.92	6.79	-864	10413.5	0.038	0.077	0.023	0.231	-0.0146	0.153
	Bh		2708.5	5770.5	1467	15625	6.57	7.74	-1242	9854.5	0.041	0.075	0.022	0.202	-0.0189	0.127
	CB		2570	5005	1712	17255	6.97	8.12	-858	12250	0.037	0.062	0.025	0.212	-0.0123	0.151
Profile 6	Ah 1	Corleone Calcarenite	1278	1657.5	1086	10048.5	5.10	5.01	-193	8391	0.025	0.033	0.021	0.201	-0.0038	0.168
	Ah 2		1080	949.6	1206	9840	6.03	4.27	126	8890.4	0.018	0.022	0.020	0.230	0.0021	0.208
	BwC		856.9	783	1045	9022	7.24	4.00	188	8239	0.012	0.020	0.014	0.226	0.0026	0.206
	Bwk		873	589.95	1195	9004	6.29	3.88	322	8414.05	0.014	0.015	0.019	0.232	0.0051	0.217
Profile 7	Ah 1	Corleone Calcarenite	1691	2749	1219	11215	5.43	5.64	-473	8466	0.031	0.049	0.022	0.199	-0.0087	0.150
	Ah 2		1715	2194	1394	12075	5.80	5.77	-322	9881	0.030	0.038	0.024	0.209	-0.0055	0.171
	Bwk		1162.5	1323	1282	10102	5.78	4.74	120	8779	0.020	0.028	0.022	0.213	0.0021	0.185
Profile 8	Ap	Corleone Calcarenite	2349	6412	3383	36075	7.09	9.31	1034	29663	0.033	0.069	0.048	0.387	0.0146	0.319
	Bh 1		2182	6300.5	3433	36395	7.45	9.62	1251	30094.5	0.029	0.065	0.046	0.378	0.0168	0.313
	Bh 2		2238	6712.5	3564	34295	7.18	9.69	1326	27582.5	0.031	0.069	0.050	0.354	0.0185	0.285
Profile 9	Ah	Corleone Calcarenite	2076	4333	1381	16920	5.35	7.96	-695	12587	0.039	0.054	0.026	0.213	-0.0130	0.158
Profile 10	Ah 1	Numidian Flysch	1235	3176	1851	24775	10.52	4.96	616	21599	0.012	0.064	0.018	0.500	0.0059	0.436
	Ah 2		1100.5	2180	1815	26635	11.99	5.40	715	24455	0.009	0.040	0.015	0.493	0.0060	0.453
	Bw		758.25	2262	1662	32535	11.76	5.74	904	30273	0.006	0.039	0.014	0.567	0.0077	0.527
	CB		463.95	2172.5	744	23280	10.41	4.58	280	21107.5	0.004	0.047	0.007	0.508	0.0027	0.461

3.3 Weathering indices

(Ca+K)/Ti: As shown in Figure 8, there are roughly two groups: Profiles 6 and 7 exhibit significantly higher ratios, ranging from 33 to 47, while all other profiles display lower values between 2.8 and 26.6. Within the low-ratio group, intra-profile variation is minimal, with the exception of Profile 10, which shows a notable increase in the CB horizon. Profile 2 exhibits the lowest index, indicating the highest degree of weathering. Despite their geographic proximity, Profiles 9 and 3 show contrasting values—26.6 and 9.7 respectively—suggesting localized differences in weathering intensity or parent material composition. In Profile 6, the Ah1 horizon shows a markedly lower ratio than its deeper horizons, hinting at increased weathering in the surface layer.

The strong contrast between Profiles 6 and 7 and the rest of the dataset suggests these soils have experienced either significantly less weathering or more recent disturbances. This interpretation is supported by data in Table 2, which shows that Profiles 6 and 7 also have notably higher $CaCO_3$ contents compared to the other profiles, which influences the outcome of the index.

(Na+K)/Ti: As becomes evident from Figure 8, this ratio exhibits substantial variation across profiles and presents a different pattern compared to the (Ca + K)/Ti index. Notably, Profile 6 displays the lowest values for this index, with a marked increase in the BwC horizon. This trend contrasts with its (Ca + K)/Ti pattern. Profiles 1, 2, and 10 also show consistently low (Na + K)/Ti ratios, indicating that these soils are more strongly weathered. In contrast, Profiles 4 and 8, along with the Ah horizon of Profile 9, show the highest ratios, suggesting comparatively less weathering.

Chemical Index of Alteration (CIA): Figure 8 shows a similar pattern to the first index, with profiles 6, 7, and 9 forming a distinct group separate from the other sites, and profiles 1, 2, and 10 exhibiting the highest degrees of weathering. Interestingly, the Ah horizons of profiles 3 (CIA = 59.8) and 9 (CIA = 39.3) display significant differences, despite similar environmental settings and close proximity. The lower CIA value for profile 9 suggests less weathered soil, which may be attributed to its slightly higher elevation and upper slope position. Overall, CIA values do not vary greatly within individual profiles. However, most show a slightly lower index in the topsoil, possibly reflecting surface processes such as organic matter input or disturbances. A notable exception is profile 10, where the index decreases sharply in the CB horizon (from 76 to 58), indicating a shift to less weathered material in the subsoil—a trend not observed in the other profiles.

Weathering index of Parker (WIP): Figure 8 reveals a pattern broadly consistent with the (Ca+K)/Ti index and the CIA, with profiles 1, 2, and 10 exhibiting lower WIP values—indicative of more advanced weathering—compared to the higher values observed in profiles 6 and 7. Unlike the previous indices, the WIP shows slightly more variation within individual profiles. In most cases, the topsoil horizons display lower WIP values, suggesting greater degrees of weathering at the surface.

Primitive mantle: Figure 9 illustrates the trace element enrichment in the soil profiles, represented by the average ratio per profile in comparison to the primitive mantle values (Sun & McDonough, 1989). Several trace elements display significant enrichment, with Rb, Th, and Pr showing values exceeding 100 times that of the primitive mantle. Profiles 1 and 2 are notably enriched in Ta, while profiles 4, 8, and 10 show elevated concentrations of Nd. In contrast, Sr and Ti exhibit much lower enrichment, with values approaching those of the primitive mantle, indicating their relative immobility or depletion. Despite some variability among individual profiles, the overall enrichment pattern remains consistent across sites. This suggests that the soils likely share a common local geological origin.

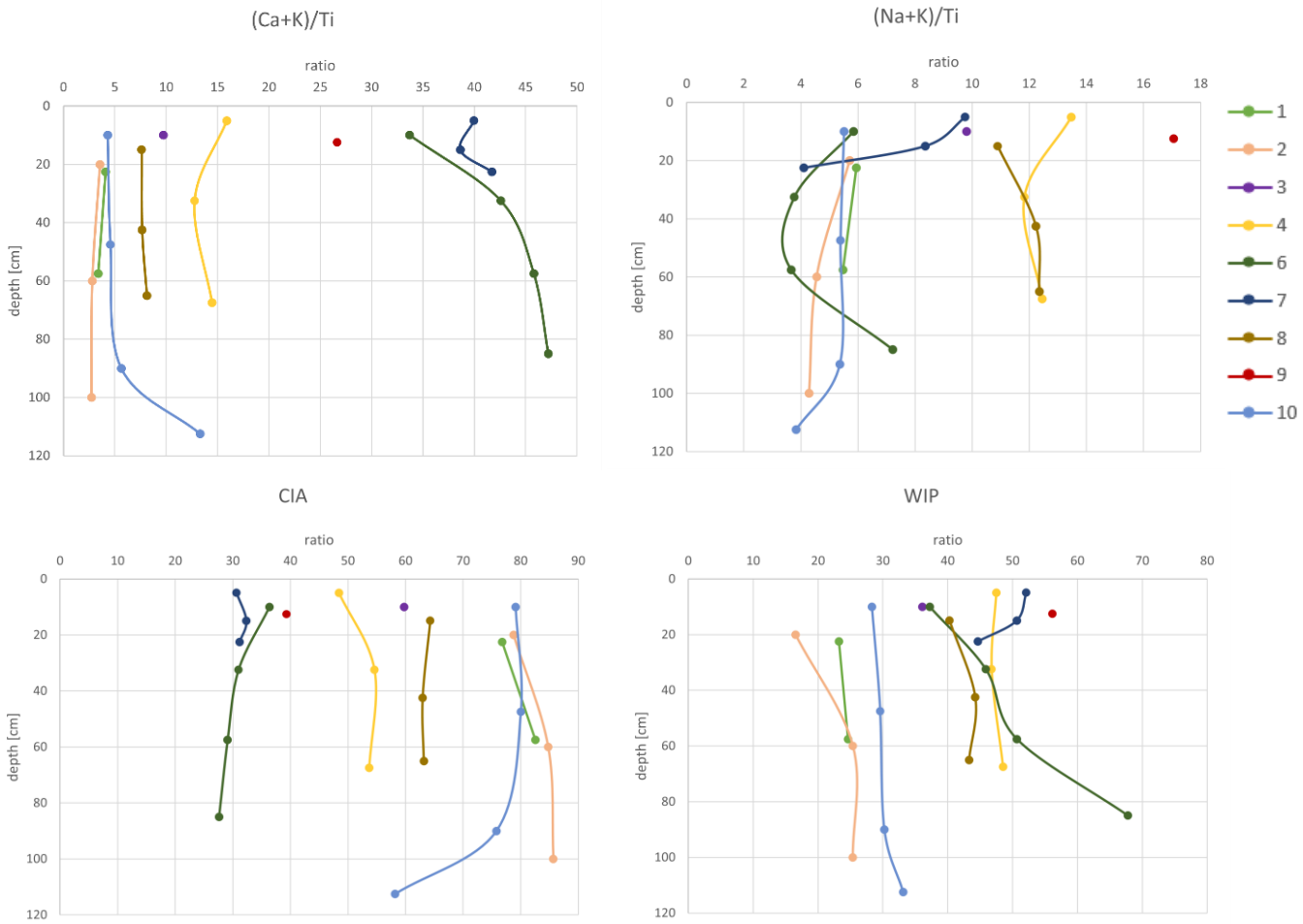

Figure 8: Weathering indices of the different soil profiles

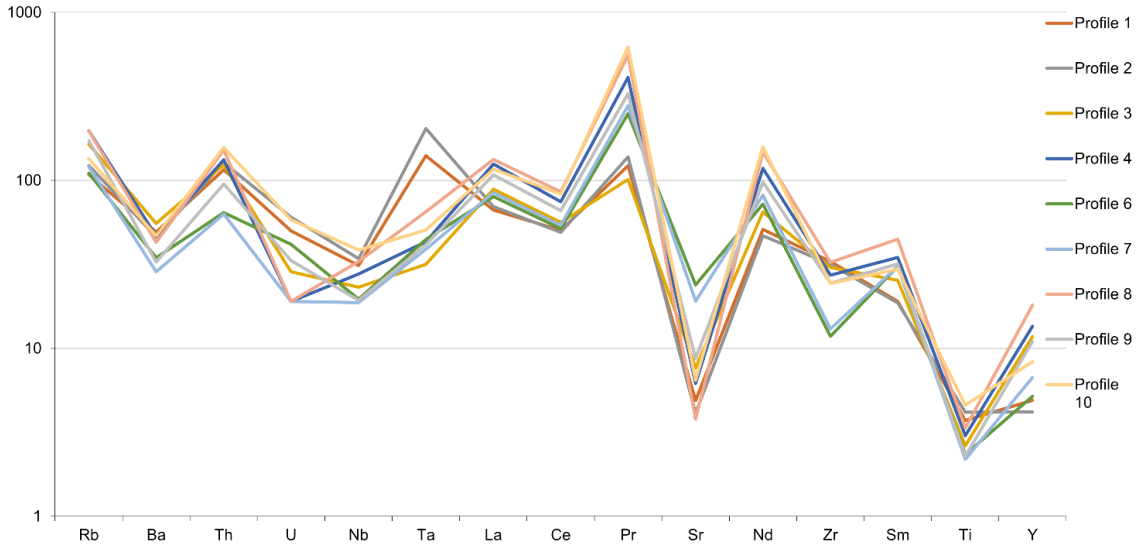

Figure 9: Measured trace elements of the soil profiles (average per profile) compared to the primitive mantle

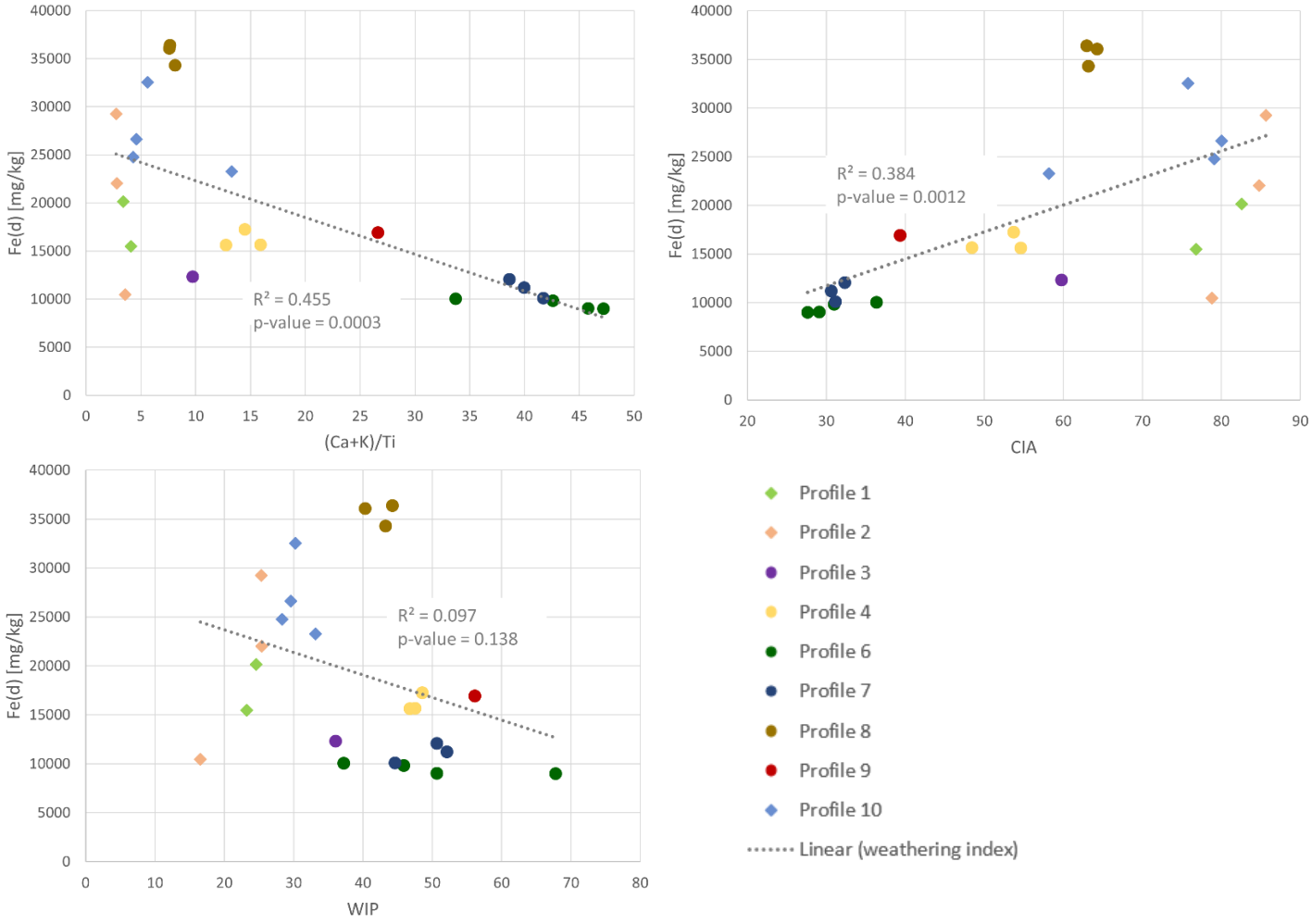

Figure 10: Dithionite extracted iron compared to the weathering indices (Ca+K)/Ti, CIA, WIP by linear regression.

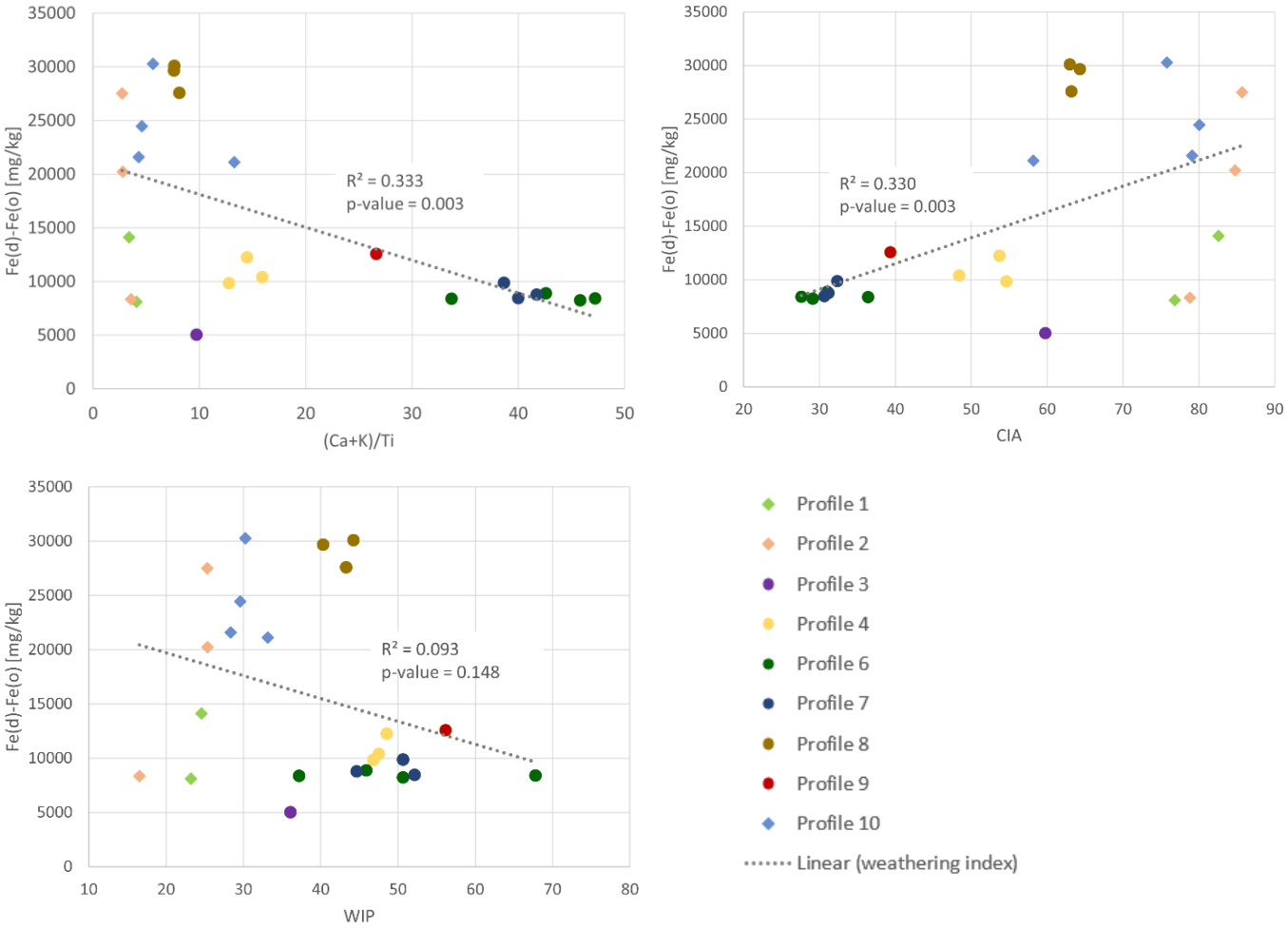

Figure 11: Crystalline Iron (Fe(d)-Fe(o)) compared to the weathering indices (Ca+K)/Ti, CIA, WIP by linear regression.

3.3.1 Comparison with oxyhydroxides

Figure 10 presents linear regressions between dithionite-extracted iron (Fe(d)) and three weathering indices. A clear trend emerges for both the (Ca+K)/Ti index and the Chemical Index of Alteration (CIA), where increased weathering correlates with higher Fe(d) content. Specifically, a decrease in the (Ca+K)/Ti index—indicative of greater weathering—is associated with an increase in Fe(d). Similarly, the CIA, which increases with progressive weathering, also shows a positive correlation with Fe(d), reinforcing the role of weathering in iron mobilization and transformation. In contrast, the Weathering Index of Parker (WIP) does not exhibit a statistically significant relationship (p-value > 0.05), although the general trend aligns with the other indices.

A similar pattern is observed when considering the crystalline fraction of iron (Fe(d) - Fe(o)) as shown in Figure 11, where the strongest correlation is again found with the (Ca+K)/Ti index, followed by a statistically significant correlation with CIA. Notably, profiles 6 and 7 cluster distinctly with both low CIA values and reduced Fe(d) - Fe(o) content, suggesting more recent disturbance or reduced weathering intensity at these sites.

3.4 Carbon fractions

Table 4 shows the different carbon fractions identified in the soil samples for the bulk samples and for the aggregate size fractions >63 µm and <63 µm. In Figure 14 these organic carbon concentrations for the three fractions are visualized, revealing no significant differences in organic carbon content between them. Figure 15 further illustrates how the total organic carbon stock in each profile is distributed across the two aggregate size fractions.

3.4.1 Carbon fractions - bulk

Total carbon, as shown in Table 4, is generally highest in the upper soil horizons. When comparing total carbon with clay content, a slight negative linear correlation can be identified, indicating that soils with lower clay content tend to have higher total carbon (see Figure 12). The summed organic carbon stock for each profile is shown in Figure 13.

The OC-content is highest in the topsoil for all profiles. Profile 4 stands out with a particularly high organic carbon concentration (6.71% in the Ah horizon). This profile is located in a forest and consequently receives a high litter input. Similarly, profiles 3 and 9, both located on La Montagna Vecchia, exhibit elevated organic carbon levels (4.8% and 5.6%, respectively). In contrast, the lowest OC concentrations (0.3–0.8%) are observed in the B to CB horizons of profiles 1, 2, and 10, all situated in Bosco della Ficuzza. The difference in OC content between these three profiles and the rest is statistically significant ($W = 121$, p-value = 0.00074). The negative correlation between organic carbon and clay content is modest but significant ($R^2 = 0.17$, p-value = 0.042).

Inorganic carbon content is generally low across all profiles (0.02–0.45%), with the notable exception of profiles 6 and 7. These two neighboring profiles show significantly higher inorganic carbon levels, with relatively low clay contents. In profile 6, inorganic carbon decreases with depth (4.05% in the BwC horizon), whereas in profile 7 it increases, reaching 4.8% in the Bwk horizon. Consistent with this, $CaCO_3$ content is negligible in all profiles except 6 and 7, with the highest concentration (40%) recorded in the Bwk horizon of profile 7.

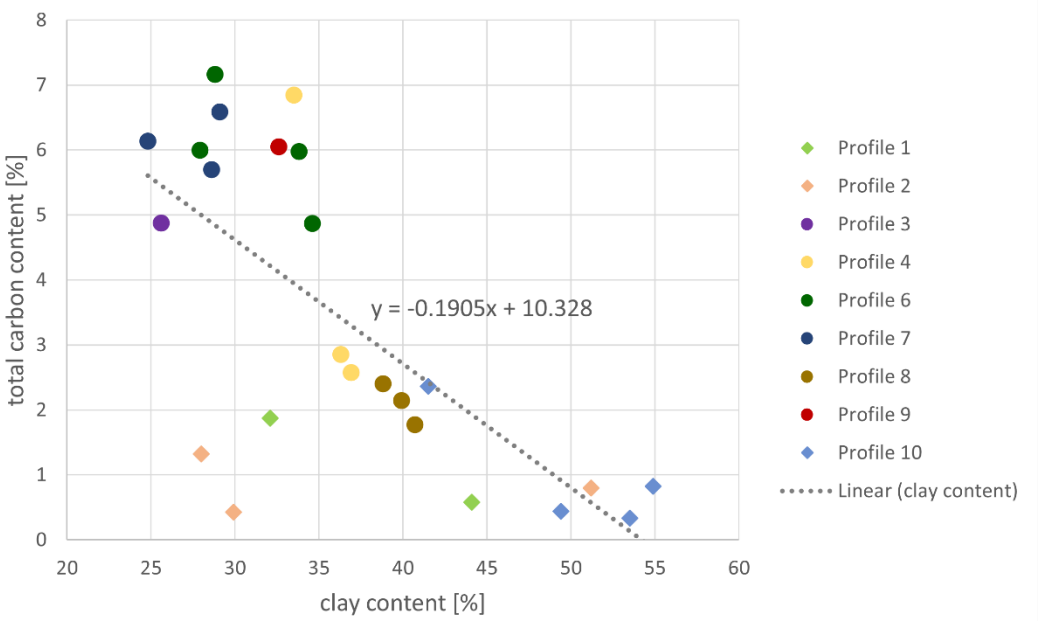

Figure 12: linear regression of total carbon content and clay content. (R2 = 0.48, p-value = 0.0002).

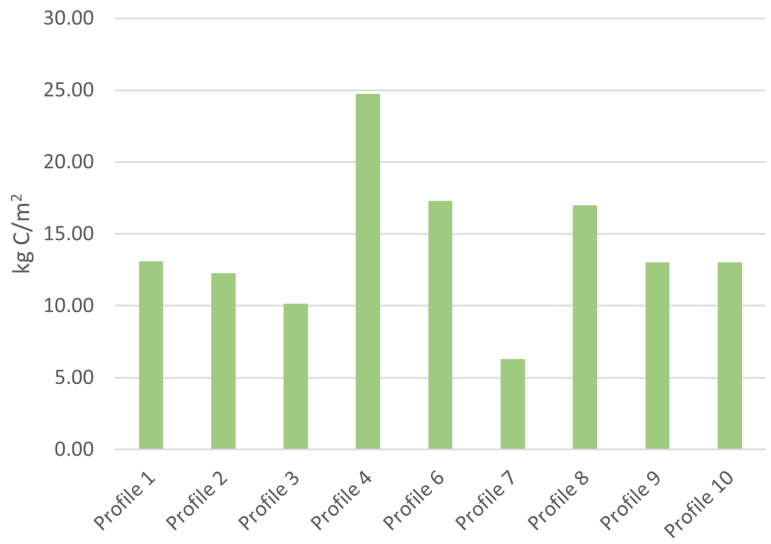

Figure 13: Organic carbon stocks in the sampled soil profiles

3.4.2 Carbon fractions - >63 µm

The organic carbon content in the >63 µm soil fraction, which includes sand and small aggregates, is on average slightly higher than in the bulk samples (median >63 µm = 1.97%, median bulk = 1.79%). As with the bulk samples, organic carbon is consistently highest in the topsoil across all profiles. However, the distribution between profiles shows slight differences. In profiles 1, 2, 3, 4, 8, 9, and 10, the organic carbon content in the >63 µm fraction is slightly lower than in the bulk samples (average >63 µm = 2.1%, average bulk = 2.18%). In contrast, profiles 6 and 7 show the opposite trend, with a

higher average organic carbon content in the >63 µm fraction (2.26%) compared to the bulk samples (1.81%). Despite these differences, the variations between fractions are not statistically significant.

Inorganic carbon content in the >63 µm fraction ranges from 0.01% to 4.32%, closely mirroring the values observed in the bulk samples. Once again, profiles 6 and 7 stand out with significantly higher inorganic carbon levels. The same trend applies to $CaCO_3$ content, which is slightly lower in the sandy fraction compared to the bulk samples, though the difference is minor and overall patterns remain consistent across profiles.

3.4.3 Carbon fractions - <63 µm

In most samples, the <63 µm fraction (fine material) contains slightly higher organic carbon concentrations than the corresponding bulk samples. However, in profiles 3, 4, 8, and 9, the organic carbon content in this finer fraction is marginally lower. Inorganic carbon content is lower in the <63 µm fraction compared to both the sandy fraction and the bulk samples, although differences are small and general trends within and between profiles remain consistent. Similarly, $CaCO_3$ concentrations are lowest in this fine fraction. As shown in Figure 15, the allocation of total organic carbon stock to the <63 µm fraction is particularly low in profiles 6 and 7, especially in comparison to the other profiles.

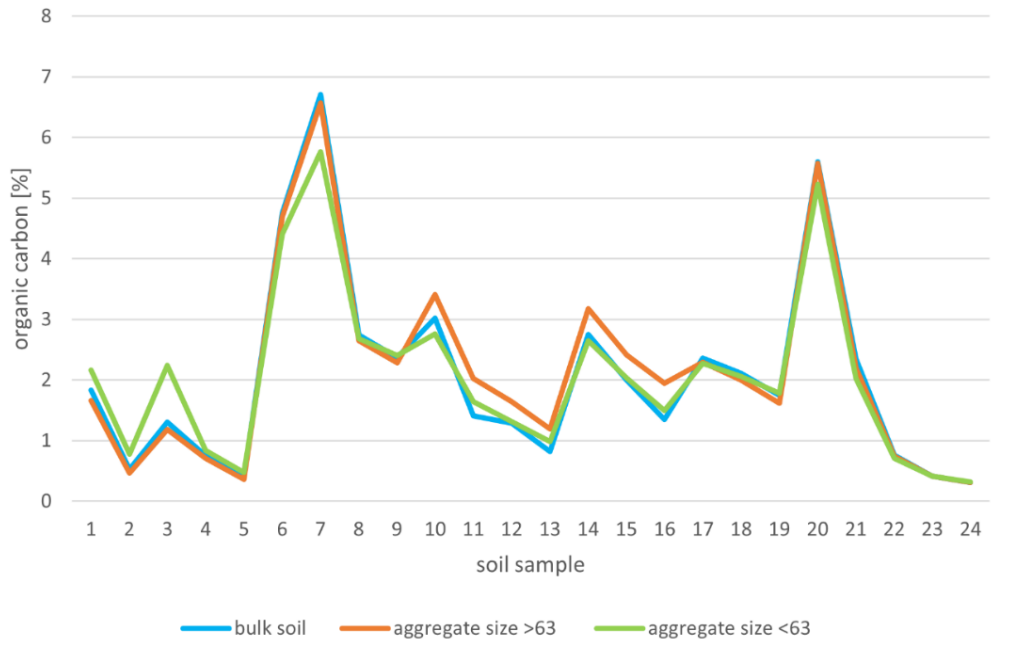

Figure 14: organic carbon concentrations for the different fractions of the soil samples (numbering: 1, 2 - profile 1; 3-5 - profile 2; 6 - profile 3; 7-9 – profile 4; 10-13 – profile 6; 14-16 – profile 7; 17-19 – profile 8, 20 – profile 9; 21-24 – profile 10)

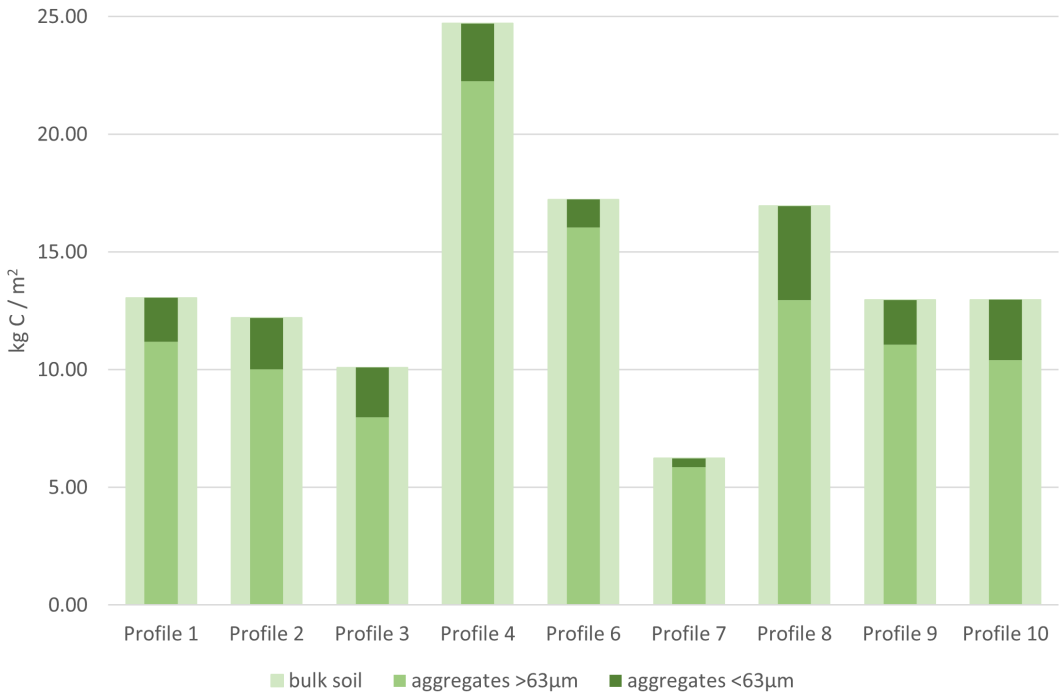

Figure 15: organic carbon stocks of the different soil fractions.

Table 4: Soil fractions and their different carbon contents

			bulk soil					aggregate size >63 µm					aggregate size <63 µm				
Site	horizon	depth cm	total C %	Corg %	Cinorg %	CaCO3 %	org. C-stock kg/m²	total C %	Corg %	Cinorg %	CaCO3 %	org. C-stock kg/m²	total C %	Corg %	Cinorg %	CaCO3 %	org. C-stock kg/m²
Profile 1	Ah	0-45	1.87	1.83	0.04	0.30	11.07	1.70	1.66	0.03	0.29	9.52	2.18	2.17	0.02	0.15	1.56
	Bwg	45-70	0.58	0.53	0.05	0.43	1.97	0.51	0.47	0.04	0.37	1.67	0.80	0.78	0.02	0.15	0.30
Profile 2	Ah	0-40	1.32	1.30	0.02	0.14	6.94	1.21	1.18	0.03	0.27	5.67	2.26	2.24	0.02	0.13	1.27
	Btg	40-80	0.80	0.75	0.05	0.42	3.21	0.74	0.71	0.03	0.22	2.88	0.86	0.84	0.01	0.12	0.33
	Cg	80-120	0.43	0.40	0.03	0.25	2.05	0.40	0.37	0.03	0.26	1.45	0.49	0.47	0.02	0.15	0.59
Profile 3	Ah	0-20	4.88	4.76	0.12	1.00	10.09	4.79	4.69	0.10	0.80	7.97	4.50	4.41	0.09	0.73	2.13
Profile 4	Ah	0-10	6.85	6.71	0.14	1.15	5.78	6.73	6.57	0.16	1.37	5.44	5.88	5.76	0.12	1.00	0.34
	Bh	10-55	2.85	2.74	0.11	0.92	13.25	2.75	2.65	0.11	0.91	11.66	2.82	2.68	0.14	1.15	1.59
	CB	55-80	2.57	2.37	0.20	1.70	5.67	2.49	2.28	0.21	1.75	5.15	2.65	2.41	0.24	2.00	0.52
Profile 6	Ah 1	0-20	7.17	3.02	4.15	34.54	5.01	7.23	3.41	3.82	31.81	4.74	6.20	2.76	3.44	28.65	0.27
	Ah 2	20-45	6.00	1.41	4.59	38.23	4.64	5.98	2.03	3.95	32.88	4.42	5.51	1.64	3.87	32.24	0.22
	Bwk	45-70	5.98	1.29	4.69	39.05	4.35	5.84	1.64	4.20	35.02	3.92	5.64	1.31	4.32	36.04	0.43
	BwC	70-100	4.87	0.82	4.05	33.73	3.23	4.86	1.19	3.67	30.57	2.95	4.88	0.99	3.89	32.41	0.28
Profile 7	Ah 1	0-10	6.59	2.75	3.83	31.95	3.65	6.54	3.18	3.36	28.04	3.45	5.18	2.65	2.53	21.05	0.20
	Ah 2	10-20	5.70	2.00	3.70	30.82	1.91	5.73	2.41	3.32	27.66	1.78	4.50	2.03	2.46	20.53	0.13
	Bwk	20-25	6.14	1.35	4.79	39.90	0.68	6.26	1.94	4.32	35.96	0.62	5.47	1.49	3.97	33.12	0.06
Profile 8	Ap	0-30	2.40	2.36	0.04	0.29	7.60	2.30	2.29	0.01	0.06	6.11	2.31	2.28	0.04	0.30	1.49
	Bh 1	30-55	2.15	2.12	0.03	0.26	4.88	2.01	2.00	0.01	0.07	3.52	2.11	2.06	0.05	0.40	1.37
	Bh 2	55-75	1.77	1.74	0.03	0.24	4.46	1.63	1.62	0.01	0.07	3.32	1.83	1.78	0.05	0.38	1.14
Profile 9	Ah	0-25	6.05	5.60	0.45	3.76	12.96	6.02	5.57	0.44	3.69	11.07	5.55	5.22	0.32	2.70	1.89
Profile 10	Ah 1	0-20	2.36	2.34	0.02	0.15	5.54	2.21	2.20	0.01	0.08	4.28	2.09	2.03	0.06	0.49	1.26
	Ah 2	20-75	0.83	0.76	0.07	0.56	0.67	0.82	0.75	0.07	0.59	0.53	0.79	0.71	0.08	0.67	0.14
	Bw	75-105	0.44	0.42	0.02	0.18	5.17	0.42	0.41	0.01	0.09	4.22	0.47	0.41	0.06	0.51	0.94
	CB	105-120	0.33	0.31	0.02	0.16	1.59	0.32	0.31	0.01	0.10	1.38	0.37	0.32	0.05	0.38	0.22

Table 5: Nitrogen, C/N and d13C values of the different size fractions

			bulk soil			aggregate size >63			aggregate size <63		
Site	horizon	depth	N	C/N	$\delta^{13}C$	N	C/N	$\delta^{13}C$	N	C/N	$\delta^{13}C$
		cm	%		‰	%		‰	%		‰
Profile 1	Ah	0-45	0.14	12.9	-26.4	0.14	11.7	-26.5	0.16	13.8	-26.2
	Bwg	45-70	0.04	14.1	-26.0	0.05	9.5	-26.1	0.05	16.0	-25.9
Profile 2	Ah	0-40	0.08	16.8	-26.8	0.08	15.2	-27.0	0.13	17.6	-26.6
	Btg	40-80	0.06	13.6	-25.9	0.07	10.1	-26.1	0.04	20.1	-25.9
	Cg	80-120	0.03	13.4	-25.9	0.05	8.1	-26.0	0.03	15.2	-25.7
Profile 3	Ah	0-20	0.43	11.2	-26.2	0.46	10.3	-26.4	0.35	12.7	-26.2
Profile 4	Ah	0-10	0.45	15.0	-26.5	0.46	14.3	-26.8	0.34	17.2	-26.3
	Bh	10-55	0.19	14.5	-25.3	0.23	11.6	-25.3	0.17	15.9	-25.0
	CB	55-80	0.18	12.9	-23.9	0.20	11.3	-23.9	0.15	16.0	-23.6
Profile 6	Ah 1	0-20	0.20	15.1	-11.5	0.22	15.8	-11.0	0.24	11.3	-14.4
	Ah 2	20-45	0.06	22.4	-8.2	0.09	23.1	-8.2	0.09	17.4	-9.8
	Bwk	45-70	0.05	28.6	-6.6	0.05	31.2	-6.5	0.06	23.1	-7.6
	BwC	70-100	0.03	26.3	-5.0	0.05	26.1	-5.1	0.04	22.8	-5.5
Profile 7	Ah 1	0-10	0.20	13.6	-12.5	0.24	13.2	-12.2	0.26	10.3	-16.3
	Ah 2	10-20	0.13	15.7	-10.3	0.16	15.4	-9.6	0.18	11.2	-14.2
	Bwk	20-25	0.07	18.5	-7.8	0.09	21.1	-7.2	0.13	11.6	-10.2
Profile 8	Ap	0-30	0.17	14.3	-27.0	0.19	12.3	-27.1	0.18	12.4	-27.0
	Bh 1	30-55	0.14	15.0	-26.6	0.17	11.8	-26.7	0.16	13.3	-26.7
	Bh 2	55-75	0.10	18.1	-26.4	0.13	12.0	-26.4	0.14	12.8	-26.5
Profile 9	Ah	0-25	0.48	11.6	-24.1	0.54	10.3	-23.9	0.47	11.2	-25.0
Profile 10	Ah 1	0-20	0.19	12.6	-27.7	0.21	10.5	-27.9	0.20	10.1	-27.9
	Ah 2	20-75	0.08	8.9	-25.1	0.11	6.9	-24.5	0.12	6.2	-25.6
	Bw	75-105	0.06	6.8	-26.0	0.09	4.4	-26.2	0.10	4.1	-26.3
	CB	105-120	0.05	6.8	-26.4	0.07	4.3	-26.5	0.09	3.8	-26.9

3.4.4 C/N ratio

The carbon-to-nitrogen (C/N) ratio offers valuable insight into nutrient availability and organic matter decomposition dynamics in soils. As presented in Table 5, C/N ratios vary notably between profiles. The lowest ratio for the bulk soil is found in profile 10 with an average of 8.8, while the highest is found in profile 6 (average: 23.1). Both profiles 3 and 9, located at La Montagna Vecchia, show low C/N ratios (profile 3: 11.2; profile 9: 11.6). Profile 6 stands out with consistently elevated C/N values across horizons, indicating lower relative nitrogen content and potentially slower organic matter decomposition. Profiles 6, 7, and 8 also exhibit an increasing C/N ratio with soil depth, primarily due to a reduction in total nitrogen content in deeper horizons. When comparing C/N ratios across different soil fractions, some variability is observed, but no consistent trend emerges. In most cases, differences between fractions are minor and not systematically related to depth or profile.

3.4.5 Isotopes

The $\delta^{13}C$ signature offers valuable insight into the origin, decomposition, and turnover of soil organic matter. Table 5 presents $\delta^{13}C$ values for all soil samples. Most bulk soil samples (profiles 1, 2, 3, 4, 8, 9, and 10) exhibit negative $\delta^{13}C$ values ranging from -27.8 to -23.9 ‰. In contrast, profiles 6 and 7 display less negative values, ranging from -12.5 to -5 ‰. This isotopic enrichment is likely attributed to the higher carbonate content in these soils. Within individual profiles, the most negative $\delta^{13}C$ are always measured in the upper soil horizons, reflecting fresher organic inputs and less decomposed material. No significant differences or consistent trends were observed between the different soil fractions.

3.5 Density fractionation

Due to methodological limitations, the attempted density fractionation of the soil samples into two density classes (>1 g/cm³ and <1 g/cm³) did not produce reliable results. The fraction with a density below 1 g/cm³ yielded less than 50 mg of material per sample, rendering subsequent analyses unfeasible. These results suggest that the majority of the soil matrix possesses a density greater than 1 g/cm³. It is therefore likely that fractionation using a liquid medium with a higher density than water would have been more effective in separating distinct soil components.

4 Discussion

4.1 Overview of carbon in soils of the Corleone Geopark region

The investigated soil profiles in the proposed Geopark region contain roughly between 1 to 6% total carbon (Table 4).

4.1.1 Inorganic carbon

The calcium carbonate content is generally low across all profiles, except for profiles 6 and 7, which exhibit the highest inorganic carbon contents. Compared to other studies from the same region, these calcium carbonate levels are exceptionally low (Egli et al., 2021). Calcium carbonates are known to buffer soil pH, which aligns with the higher pH values observed in profiles 6 and 7. Additionally, carbonates can influence the solubility of organic matter and nutrient availability (Zhou et al., 2019). While the presence of calcium carbonates is influenced by both parent material and weathering processes (Weil et al., 2017), parent material alone does not seem to explain the observed variations. Both profiles 6 and 7 have formed on Corleone Calcarenite, but so have the profiles 3, 8, and 9 which exhibit low inorganic carbon contents. This suggests that weathering degree plays a more significant role than parent material in determining inorganic carbon values. Supporting this, Egli et al. (2024) found that Kaolinite formation resulting from weathering of parent material in the same region was associated with high Ca losses. The weathering indices as shown in Figure 8 indicate least weathering for the profiles 6 and 7, which corresponds to those findings.

Furthermore, Egli et al. (2024) found that the proportion of pedogenic carbonates within total inorganic carbon correlates positively with the weathering indices, showing that with a higher weathering degree, the proportion of secondary carbonates increased (Egli et al., 2024). It is very probable that the same conclusion can be made for the investigated soil profiles. While no $\delta^{13}C$ values of the original carbonates were calculated, the $\delta^{13}C$ values of the bulk soil are comparable to the ones in the study, along with the inorganic carbon contents (as shown in Table 4 and Table 5). Topsoils in profiles with almost no inorganic C (less than 0.5%) have average $\delta^{13}C$ values of -26.38 ± 1.06 ‰, closely matching the average of 26.36 ± 0.60 ‰ reported by Egli et al. (2024). Conversely, profiles 6 and 7, which contain more inorganic carbon, exhibit bulk soil $\delta^{13}C$ values averaging -8.8 ± 2.50 ‰, attributable to the higher $CaCO_3$ content. This leads to the conclusion that similarly to the mentioned study, the $\delta^{13}C$ signals of topsoil of the profiles 1 to 4 and 8 to 10 are determined by decomposed C3 plants (C3 plants in Mediterranean regions exhibiting on average -27 ‰ $\delta^{13}C$ (Kohn, 2010)) and secondary carbonates. Due to the arid to semi-humid conditions in Sicily the formation of secondary carbonates is enhanced, contributing to the sequestration of carbon (Batool et al., 2024; Egli et al., 2021).

4.1.2 Organic carbon

The measured and calculated soil organic carbon (SOC) contents range from 0.3 to 6.7%, with the highest values consistently found in the upper horizon of the profiles. This can be attributed to higher input of organic carbon from litter and root systems, which is typical for most soils (Edwards, 2024; Zhao et al., 2021). Profile 4, located in a forested area, exhibits the highest organic carbon stock, likely due to increased litter input by leaves and less human impact. This corresponds to findings by Six et al. (2002) who found that forested soils stored more SOC than agricultural soils, especially in the A-horizon. A result they connect to aggregation within the soils (Six, Callewaert, et al., 2002).

To gain insight into the distribution of SOC fractions, density fractionation can be used to separate the labile particulate organic matter (POM) from the rest of the soil (Lavallee et al., 2020). However, due to time constraints, a simplified fractionation method using water at a density of 1 g/cm³ was applied. This method proved ineffective at fully separating POM from the rest of the soil. Research suggests that using a denser liquid with a density up to 1.85 g/cm³ provides more reliable separation results (Mastrolonardo et al., 2013; Viret & Grand, 2019; Zollinger et al., 2013). Consequently, organic carbon fractions were instead identified through aggregate size fractionation. The resulting carbon fractions are shown in Figure 14 and Figure 15. Interpretation of these fractions leans on established findings: smaller particles, such as clays, have a larger surface area and greater capacity to stabilize organic carbon, associating MAOM/MOC with the fraction <63 µm (Egli et al., 2007). Conversely, coarser particles, in this case the fraction >63 µm, are typically linked to POM and POC, which have higher turnover rates due to greater accessibility to microbes (Viret & Grand, 2019). When comparing the organic carbon contents of the two grain size fractions with the bulk soil, no clear trends emerge, as the concentrations across the three measurements are similar. Yet the assessment of other soil characteristics can provide insights into the organic carbon sequestration and storage within the investigated soils.

4.2 Chemical weathering and mineral composition of the soil and its effect on soil organic carbon

Weathering of soils and parent material are an important part of the global carbon cycle. Microbial mineralization along with inorganic carbon weathering and rhizosphere respiration leads to a release of CO_2 into the atmosphere, resulting in a short-term carbon storage while the microbial decomposition products may bind to soil minerals or oxyhydrates, stabilizing them for long periods of time (Smith et al., 2015). Different studies have found that soils with higher clay contents show higher rates of stabilizing organic carbon (Hassink, 1997; Jobbágy & Jackson, 2000; Six, Conant, et al., 2002; Smith et al., 2015; Wiesmeier et al., 2019).

4.2.1 Clay/ grain size

The grain size distribution of the investigated soils aligns with results from previous studies in the region (Egli et al., 2024), with high sand contents, partly high amounts of clay, and silt portraying the smallest fraction. By measuring the carbon contents of soil fractions larger and smaller than 63 µm, the distribution of organic carbon between coarser particles and aggregates versus finer particles can be assessed. It is important to note that the <63 µm fraction includes not only clay particles (up to 2 µm) but also silt (Weil et al., 2017). Similarly, the >63 µm fraction may still contain clay particles trapped within aggregates that were not fully broken up during dry sieving. Research by Hassink (1997) demonstrated that a 60 µm cut-off effectively distinguishes between carbon storage in coarse and fine fractions. Yet the study used a different method for sieving, breaking aggregates beforehand (Hassink, 1997). The research showed that the finer fraction (<60 µm) typically supports more stable, long-term carbon storage than the coarser fraction (>60 µm). Wiesmeier et al. (2019) confirm that soil texture may be the best indicator for assessing SOC storage capacity over a large scale.

Organic carbon decomposition occurs faster in sandy soils than in clay-rich soils, where carbon is better protected from microbial activity (Six et al., 2001). Clay minerals promote carbon stabilization through their large surface area and pH-dependent surface charge, which enhance carbon sorption and limit decomposition (Beare et al., 2014; Singh et al., 2018). As seen in Table 4 and Figure 14, no significant differences in OC contents were observed between the two size fractions. On average all three soil fractions contain 2.1% of OC (bulk: 2.1 ±1.60%, >63 µm: 2.1±1.58%, <63 µm: 2.1±1.39%). Summing this up into organic carbon stock, more variations are visible (see Figure 15). In most cases, the larger fraction (>63 µm) holds a significantly higher proportion of the organic carbon stock compared to the smaller fraction (<63 µm). Nevertheless, the fine fraction still retains a relevant portion, particularly in samples with higher clay content (f.i. profile 8). Generally, samples with higher bulk carbon also display greater carbon distribution across both fractions. The assumption that organic carbon in the >63 µm fraction belongs exclusively to the labile POC pool, while carbon in the <63 µm fraction represents the stable MOC pool, seems too simplistic considering these results. While finer particles are often linked to more stable carbon pools (Hassink, 1997), some carbon in the coarser fraction may also belong to the stabilized MOC pool. Previous studies suggest that SOC can accumulate within coarse aggregates, protecting organic carbon from rapid decomposition (Barbera et al., 2012; Singh et al., 2018; Six, Callewaert, et al., 2002).

The increasing clay content (up to 2 µm) in the bulk soil correlates with a decrease in organic carbon content (linear regression, $R^2 = 0.17$, $p < 0.05$). Profile 10, which has the highest clay content among the investigated profiles, shows the lowest organic carbon content and stocks per horizon, particularly in the deeper soil layers (0.32–0.76% OC). This contradicts previous research, as it has been found that deeper soil layers typically contain a higher proportion of stable MOC (Mainka et al.,

2022). However, the data presents inconsistencies, as profiles 1 and 2 exhibit elevated organic carbon content in the fine fraction of their B-horizons, potentially due to clay accumulation in these horizons (Weil et al., 2017). Profiles 3 and 9, from La Montagna Vecchia, contain the highest sand content (60.9% and 56.4%, respectively) and display relatively high organic carbon content in the coarser fraction, suggesting a more labile carbon pool. Despite their shallow depth, these profiles also show high total carbon stocks, with a relevant portion stored in the finer fraction (<63 µm). Overall, the relationship between grain size and SOC appears complex and less predictable than expected. Research indicates that the correlation between clay + silt content and SOC is often nonlinear (Georgiou et al., 2022).

4.2.2 weathering indices

The weathering indices indicate that soil profiles 1, 2, and 10 are the most weathered, while profiles 6 and 7 are the least weathered (Figure 8). A low degree of weathering suggests dynamic soil conditions and frequent disturbances (Egli et al., 2024). Consistent with the findings of Egli et al. (2024), the soils with the lowest weathering degree also show the highest $CaCO_3$ and inorganic carbon contents. Profile 7 is rather shallow (25 cm) compared to the more deeply developed profile 6 (100 cm) just a few meters lower down the hill. This likely reflects disturbance from erosion at site 7 and subsequent deposition/accumulation at site 6. The rather high C/N ratio in the B-horizon of these soils (24.5 ± 4.3) additionally hints at degradation and loss of nitrogen, leading to incomplete organic matter decomposition (Weil et al., 2017).

Similar erosion/accumulation processes may explain the differences between profiles 3 and 9 at La Montagna Vecchia. Profile 9 shows less weathered soil compared to profile 3, which lies a few meters further down the slope. This sample site is exposed to erosion due to sparse vegetation and its location at approximately 1000 m.a.s.l. The area is an archaeological site and was inhabited and intensively used already 3000 years ago (Spatafora, 1996).

The most weathered soils are relatively deep and appear to have experienced less disturbance from erosion or other dynamic processes. This is particularly evident in soils formed on Numidian Flysch (profiles 1, 2, and 10), which seem to have undergone prolonged and uninterrupted pedogenesis. The most weathered soils show relatively high clay contents, suggesting a more stable carbon pool in these soils. It was also found that the weathering of glauconite and other minerals in the calcarenites of Corleone contributes to the formation of secondary minerals such as kaolinite and smectite (Egli et al., 2024), which enhances the soil's ability to stabilize organic carbon (Beare et al., 2014; Singh et al., 2018). However, profile 4, which has the highest organic carbon stock, is only moderately weathered (average CIA: 52.2 ± 2.73). This profile lies within a deciduous forest, where high litter input likely contributes to its elevated SOC stock, despite the moderate weathering status.

4.2.3 Oxyhydroxides

Weathering processes lead to the formation of secondary minerals, including oxyhydroxides such as gibbsite (Al-oxyhydroxide) and goethite (Fe-oxide) (Wiesmeier et al., 2019). Profile 8, a Vertisol used as agricultural grassland, exhibits the highest iron content among the studied soils. This profile also shows relatively high organic carbon content and stock (16.95 kg C/m²) and moderate to high weathering intensity. Egli et al. (2024) demonstrated that glauconite weathering within Corleone Calcarenites enriches soils with oxyhydroxides, significantly contributing to soil organic carbon (SOC) sequestration. The investigated soils exhibit high Fe(o) and Fe(d) contents (Table 3), indicating active weathering. These values are comparable to those reported by Egli et al. (2024), who found that glauconite content positively correlated with both oxalate- and dithionite-extractable Fe and Al ($p < 0.05$), underscoring glauconite weathering's role in pedogenic Fe formation. Dithionite extraction targets more stable, crystalline Fe minerals that typically form over longer timescales and are closely linked to soil development processes (Borggaard, 1988; Cornell & Schwertmann, 2003). The correlation between dithionite-extracted Fe and weathering (Figure 10) suggests that in the investigated region, weathering processes actively contribute to oxyhydroxide formation rather than only reflecting passive enrichment. Similarly, the well-crystallized iron oxides represented by Fe(d) - Fe(o) correlate positively with the weathering indices (Figure 11). Soil components such as Fe-oxides, Al-oxides, and hydroxides are known to have high specific surface areas, enhancing their capacity for SOC storage (Wiesmeier et al., 2019). The positive correlation between Fe(d) and Fe(d) - Fe(o) with clay content (Figure 6) further emphasizes the formation of secondary minerals. Clay minerals with expandable surfaces, such as smectite, form stable complexes with organic material, improving SOC retention (Egli et al., 2024; Wiesmeier et al., 2019). Fe(o) also correlates positively with organic carbon stock ($R^2 = 0.32$, $p < 0.05$; Figure 5). However, no significant correlations between other forms of the investigated hydroxides and organic carbon were found.

4.2.4 Effects of the parent material

Soil formation in the Corleone region is influenced by parent material, with the investigated soils developing on Corleone Calcarenites or Numidian Flysch. Certain oxyhydroxide ratios reveal distinct differences between these parent materials. The ratio (Fe(d)−Fe(o))/Fe(t) (Table 3) is significantly higher in Profiles 1, 2, and 10 compared to the other profiles formed on Corleone Calcarenite ($W = 2$, $p < 0.01$). This suggests these soils contain a greater proportion of stable iron minerals, indicating mature, well-drained soils — consistent with the weathering patterns discussed in 4.2.2. Despite their high oxyhydroxide content, these profiles (1, 2, and 10) have the lowest organic carbon contents in their B – CB horizons (0.3 – 0.8%). This difference is statistically significant ($W = 121$, $p < 0.01$). Such low SOC values are surprising, as literature indicates that oxyhydroxides — particularly iron and

aluminum — are generally effective at stabilizing soil organic matter and enhancing carbon retention in weathered and clay-rich soils (Egli et al., 2021, 2024; Wiesmeier et al., 2019).

This unexpected result suggests that other factors are influencing SOC dynamics. Corleone Calcarenites are limestones enriched in glauconite, which likely modifies weathering conditions and mineral formation in this region (Egli et al., 2024). In contrast, Numidian Flysch is composed predominantly of quartzarenites interbedded with mudstones (Johansson et al., 1998). While the soils on Numidian Flysch have experienced more intense weathering and oxyhydroxide accumulation, the presence of glauconite in Corleone Calcarenites may enhance SOC stabilization through the formation of mineral-organic complexes. These complexes protect organic matter from microbial decomposition, potentially contributing to SOC accumulation (Egli et al., 2021, 2024).

Additionally, inorganic carbon content is significantly higher in soils formed on Corleone Calcarenites than in those on Numidian Flysch ($W = 122$, $p < 0.01$). This likely adds to the overall carbon storage capacity in the region.

4.3 Distribution of SOC in the Corleone region

Following these findings, some conclusions on influences of soil type and land use on soil organic carbon in the Corleone region can be drawn.

4.3.1 Soil type

Different soil types were identified among the nine soil profiles. The results do not allow for a clear distinction of SOC stocks between these soil types. Yet the two Vertisols exhibit higher carbon stocks than most other profiles (profile 4: 24.7 kg C/m^2, profile 8: 16.95 kg C/m^2). This might be related to the higher clay content found in these profiles, which is typical for Vertisols (IUSS Working Group WRB, 2022). While profile 4 may receive more organic C through forest litter input, profile 8 is characterized by high Fe-oxyhydroxide contents, contributing to increased SOC accumulation. The profiles 1, 6, 7, and 10 were classified as Cambisol but no correlations between SOC content and this soil type are identifiable, hinting at other factors being more influential to SOC distribution in the region. However, profiles 6 and 7, both Calcaric Cambisol contain high $CaCO_3$ contents with low proportions of organic carbon stored in the finer soil fraction relative to the coarser fraction. These results might suggest that these soil profiles store little MOC and contain more labile carbon. Yet Calcium carbonate is known to stabilize soil aggregates, with calcium playing a crucial role in SOC stabilization (Clough & Skjemstad, 2000; Li et al., 2024; Wiesmeier et al., 2019). Research by Clough & Skjemstad (2000) demonstrated that OC in calcareous soils is better protected from degradation by photo-oxidation compared to non-calcareous soils. This Ca bridge effect is described in multiple

studies (Fornara et al., 2011; Li et al., 2024; Six et al., 2004). Profile 10, characterized by high clay content and deeper soil layers, exhibited the lowest SOC stocks. The profiles 3 and 9, lying close to each other, were identified as Leptic Chernic Phaeozem and exhibit both relatively large total organic carbon contents (4.8% and 5.6%). This soil type is defined by a dark, humus-rich topsoil with a shallow profile, characterized by leaching. The profiles have high sand contents and relatively high SOC concentrations in the coarser fraction, suggesting a more labile carbon pool. This demonstrates that soil type, particularly clay and sand content do influence SOC distribution and stability.

4.3.2 Effects of land use

Land use plays a significant role in determining SOC content and composition. Particulate organic matter (POM) or particulate organic carbon (POC) is particularly sensitive to land-use changes, tillage, and climatic shifts, as it is directly influenced by organic matter inputs (Lavallee et al., 2020). Additionally, anthropogenic activities and disturbances can impact soil formation, altering soil complexity and development (Phillips, 2017). Studies on Mediterranean soil formation have demonstrated a close interdependence between soil development and landscape evolution (Lin, 2011; Raimondi & Pirrone, 2020). Ancient human activity has also left lasting imprints on soil profiles, influencing their development over time (Egli et al., 2024). Practices such as deforestation, livestock grazing, and early irrigation have contributed to increased erosion rates and consequently influenced SOM accumulation (Quijano et al., 2017).

Forested areas, such as Profile 4, exhibit high SOC stocks, which aligns with findings by Six et al. (2002) that forested soils enhance carbon retention through increased litter input and improved aggregation. Notably, the SOC stock in Profile 4 is predominantly composed of POC, suggesting a more labile carbon pool that is directly influenced by recent organic matter inputs (Lavallee et al., 2020). While forest soils typically show higher SOC contents (Li et al., 2024; Six, Callewaert, et al., 2002; Wiesmeier et al., 2019), it remains uncertain whether the distribution of carbon fractions observed in Profile 4 is directly linked to land use. Contrasting evidence from temperate regions in China has shown that forests tend to store more SOC as mineral-associated organic carbon (MOC) compared to grassland or cropland (Li et al., 2024).

Profiles 3 and 9, which were historically subjected to intensive land use (Spatafora, 1996) and are now used as pasture, also exhibit relatively high SOC stocks, especially given their shallow soil depth. Along with Profiles 1, 2, and 10 — which are located in a protected agroforestry area — these two sites lie in regions protected from intensive cultivation. The limited disturbance in these areas likely contributes to the observed high weathering indices, which may enhance SOC accumulation and stabilization (Beare et al., 2014; Singh et al., 2018). However, despite being in protected areas, Profiles 3 and 9 are located on crest and shoulder slopes, making them more vulnerable to erosion.

Egli et al. (2024) noted that soils in such exposed positions tend to be less developed, with shallower profiles due to erosion. The combination of protection from intensive land use and erosion risks may explain the observed SOC patterns. While the stable conditions in protected areas promote pedogenesis, the limited organic input in these regions may restrict substantial SOC accumulation. This may account for the relatively low SOC contents in Profiles 1, 2, and 10 despite their favorable clay and iron mineral content.

It was shown that more recent human activities like plowing, synthetic fertilizers and irrigation have disrupted natural soil profiles and reduced SOC content in intensively farmed areas (Egli et al., 2024). In contrast to this, Profile 8 — an agricultural site — shows moderate to high SOC values, likely due to the presence of grassland vegetation and periodic organic material input. At this site, 24% of the total organic carbon stock is stored in the <63 µm soil fraction, suggesting a more stable and long-term carbon pool. This stability is likely linked to the site's high clay content, which enhances SOC protection and retention.

4.4 Soil organic carbon sequestration potential

SOC stabilization offers significant potential for climate change mitigation, as higher carbon stocks in soils can reduce atmospheric CO_2 levels. MOC is particularly important for long-term carbon sequestration (Hassink, 1997; Jobbágy & Jackson, 2000; Six, Conant, et al., 2002; Smith et al., 2015; Wiesmeier et al., 2019), especially with a deeper allocation of OC in the soil profile, especially when carbon is stored deeper in the soil profile (Laban et al., 2018).

In this study, Profiles 4 and 8 displayed higher carbon stocks in deeper soil horizons, indicating a more stable SOC pool. However, the more labile POC fraction also plays a crucial role in supporting soil health and short-term carbon cycling (Lavallee et al., 2020). SOC accumulation is influenced by a complex interplay of parent material, land use, and environmental factors. While this study does not investigate fire events, they too are recognized as significant drivers of SOC dynamics in Mediterranean environments (Mastrolonardo et al., 2013). Soils formed on Corleone Calcarenites, enriched with glauconite, show strong potential for SOC stabilization due to their mineralogical properties. Glauconite-rich soils promote mineral-organic complex formation, which protects organic matter from microbial decomposition. This aligns with findings by Egli et al. (2024), who report an average SOC stock of 16.5 kg C/m² in Corleone glauconites — considerably higher than SOC stocks typically reported for Mediterranean soils.

4.4.1 Comparison of SOC stocks in the mediterranean and globally

SOC stocks in the Mediterranean are generally lower than the global average, particularly in topsoil layers (FAO, 2025; Fernandes et al., 2020; Jobbágy & Jackson, 2000; Rodeghiero et al., 2011; Scharlemann et al., 2014). Globally, SOC stocks are estimated at around 1500 Pg C, with the largest reservoirs found in northern latitudes and permafrost regions (Scharlemann et al., 2014).

In Mediterranean climates, SOC values typically range between 2.5–4.5 kg C/m² for the entire soil profile (Quijano et al., 2017), or 5.87 ± 1.56 kg C/m² in the upper 30 cm of agricultural pastures (Funes et al., 2019). In Spain, reported SOC stocks range from 3.1 ± 1.0 to 4.3 ± 2.9 kg C/m² (Willaarts et al., 2016). Compared to these values, the Corleone soils show a higher carbon sequestration potential, as evidenced by their relatively elevated SOC stocks (Table 4). This reinforces the role of glauconite-enriched soils in stabilizing and retaining organic carbon. Nevertheless, land use practices, topography, and organic matter inputs remain key factors in determining SOC accumulation.

4.4.2 Future implications (land management)

Increasing SOC stocks is crucial not only for climate change mitigation but also for enhancing soil quality and ecosystem resilience. Forested and grassland soils generally maintain higher SOC stocks than croplands, a pattern reflected in the Corleone region (Wiesmeier et al., 2019). In this study, Profile 4, located in a forested area, exhibited the highest SOC stocks, largely consisting of the labile POC fraction. While POC is sensitive to land-use changes, its rapid cycling also supports nutrient availability and soil fertility. Conversely, profiles in erosion-prone and agricultural areas displayed lower SOC stocks, aligning with findings that intensive land use reduces SOC retention. Soils degraded by intensive agriculture can lose 20 to 80 tons of carbon per hectare (Lal, 2004), while emissions from land cover change are the second-largest anthropogenic carbon source released into the atmosphere (Scharlemann et al., 2014). The results of this study further support this pattern, with erosion-exposed profiles like Profile 7 showing reduced SOC stocks and signs of limited soil development.

To improve SOC retention in the Corleone region, sustainable land management strategies such as organic amendments, reduced tillage, and cover cropping should be promoted fractions (Autret et al., 2016; H. H. Gerke et al., 2016; Scharlemann et al., 2014). These practices are known to enhance both POC and MOC fractions, improving short-term carbon cycling and long-term sequestration. Encouraging soil aggregation, minimizing erosion, and integrating organic material inputs could further improve SOC retention in this region (Álvaro-Fuentes et al., 2009; Autret et al., 2016). Increasing clay content may further stabilize SOC, particularly in areas with favorable mineralogical conditions like those found in Corleone soils (Egli et al., 2021). More recently sustainable land management practices have been recommended for vulnerable soils in the region, with specific guidelines for grazing and vegetation cover, hoping to protect SOC stocks (Raimondi & Pirrone, 2020).

4.5 Limitations and future research

While the methods and results of this study are based on scientific approaches and provide valuable insights into the distribution and stabilization of SOC in the Corleone region, some difficulties and limitations should be acknowledged. Fieldwork was successful, but the manual work of digging profiles is time consuming and limited the study to nine soil profiles. This relatively small samples size limits the regional representativeness of the findings and reduces statistical significance. Also, no seasonal variabilities, which may influence organic matter input and SOC turnover are accounted for, as all samples were taken within the same week of April.

During the lab work, there were especially difficulties with the density fractionation technique. Water was used as a separation liquid, where a liquid with higher density would have better separated POM from the rest of the soil. The resulting carbon fractions identified in chapter 3.4 may not accurately reflect the true SOC pools.

Future research could focus on increasing the number and diversity of sampling sites and integrate seasonal sampling to account for temporal variation. Applying a more advanced fractionation technique and mineralogical analyses would enhance the understanding of SOC dynamics in the region. Additionally, radiocarbon dating could offer valuable insights into weathering, carbon turnover rates and anthropogenic influences.

5 Conclusion

The aim of this thesis is to assess the organic carbon stocks within the projected Corleone Geopark region and relate these to soil types, land use and other influential factors. The results of field and lab work contribute to filling knowledge gaps on soil carbon in the region and answering the research questions presented in 1.5. The investigated soil profiles reveal that land use significantly influences soil carbon content and distribution within the Corleone Geopark region. Profile 4, located in a forested area, consistently exhibits the highest organic carbon stocks. Conversely, profiles situated in agricultural areas, such as Profile 8, demonstrate moderate to high organic carbon contents, suggesting that while cultivation may reduce SOC in some cases, the presence of grassland vegetation and periodic input of organic material can sustain carbon stocks to a certain degree. Profiles from erosion-prone locations, such as Profile 7, reveal lower organic carbon stocks, indicating that land management practices and exposure to environmental disturbances can strongly influence carbon retention. The limited disturbance in protected areas generally favors SOC stability but may limit carbon inputs, particularly in deeper horizons. The relatively low SOC in some profiles suggests that without consistent organic input, even stable environments with favorable iron mineral content may struggle to accumulate significant carbon reserves. Parent material is shown to correlate with oxyhydroxide content and soil organic carbon in the lower soil with profiles on Numidian Flysch exhibiting significantly lower SOC contents than from Corleone Calcarenite. The presence of glauconitic calcarenite appears to influence SOC dynamics through its contribution to weathering processes and secondary mineral formation. Profiles developed on Corleone Calcarenite exhibited variable SOC contents, with weathering playing a critical role in stabilizing carbon. Weathering processes release Ca ions, promoting secondary carbonate formation, which can enhance carbon sequestration in arid to semi-humid environments. Additionally, glauconite weathering enriches soils with oxyhydroxides, which provide large surface areas for organic carbon stabilization. This is particularly evident in Profile 8, where the high iron content correlates with increased SOC stock, suggesting that oxyhydroxide formation contributes to improved SOC stability. The observed trends highlight the importance of sustainable land management practices that minimize erosion and promote organic input, particularly in vulnerable landscapes. Implementing practices such as afforestation, conservation tillage, and strategic vegetation cover can improve SOC retention while mitigating carbon losses through erosion. Future research could investigate the long-term impacts of specific land use changes on SOC stability and overall carbon sequestration potential in this region.

6 Bibliography

Albaladejo, J., Ortiz, R., Garcia-Franco, N., Navarro, A. R., Almagro, M., Pintado, J. G., & Martínez-Mena, M. (2013). Land use and climate change impacts on soil organic carbon stocks in semi-arid Spain. *Journal of Soils and Sediments*, *13*(2), 265–277. https://doi.org/10.1007/s11368-012-0617-7

Álvaro-Fuentes, J., López, M. V., Arrúe, J. L., Moret, D., & Paustian, K. (2009). Tillage and cropping effects on soil organic carbon in Mediterranean semiarid agroecosystems: Testing the Century model. *Agriculture, Ecosystems & Environment*, *134*(3), 211–217. https://doi.org/10.1016/j.agee.2009.07.001

Autret, B., Mary, B., Chenu, C., Balabane, M., Girardin, C., Bertrand, M., Grandeau, G., & Beaudoin, N. (2016). Alternative arable cropping systems: A key to increase soil organic carbon storage? Results from a 16 year field experiment. *Agriculture, Ecosystems & Environment*, *232*, 150–164. https://doi.org/10.1016/j.agee.2016.07.008

Barbera, V., Poma, I., Gristina, L., Novara, A., & Egli, M. (2012). Long-term cropping systems and tillage management effects on soil organic carbon stock and steady state level of C sequestration rates in a semiarid environment. *Land Degradation & Development*, *23*(1), 82–91. https://doi.org/10.1002/ldr.1055

Basilone, L. (2011). Geological Map of the Rocca Busambra-Corleone region (western Sicily, Italy): Explanatory notes. *Italian Journal of Geosciences*, *130 (2011) f.1*. https://doi.org/10.3301/IJG.2010.17

Batool, M., Cihacek, L. J., & Alghamdi, R. S. (2024). Soil Inorganic Carbon Formation and the Sequestration of Secondary Carbonates in Global Carbon Pools: A Review. *Soil Systems*, *8*(1), Article 1. https://doi.org/10.3390/soilsystems8010015

Bazan, G., Marino, P., Guarino, R., Domina, G., & Schicchi, R. (2015). Bioclimatology and Vegetation Series in Sicily: A Geostatistical Approach. *Annales Botanici Fennici*, *52*(1–2), 1–18. https://doi.org/10.5735/085.052.0202

Beare, M. H., McNeill, S. J., Curtin, D., Parfitt, R. L., Jones, H. S., Dodd, M. B., & Sharp, J. (2014). Estimating the organic carbon stabilisation capacity and saturation deficit of soils: A New Zealand case study. *Biogeochemistry*, *120*(1), 71–87. https://doi.org/10.1007/s10533-014-9982-1

Bonar, A. L., Soreghan, G. S., & Elwood Madden, M. E. (2023). Assessing Weathering, Pedogenesis, and Silt Generation in Granitoid-Hosted Soils From Contrasting Hydroclimates. *Journal of Geophysical Research: Earth Surface*, *128*(7), e2023JF007095. https://doi.org/10.1029/2023JF007095

Borggaard, O. K. (1988). Phase Identification by Selective Dissolution Techniques. In J. W. Stucki, B. A. Goodman, & U. Schwertmann (Eds.), *Iron in Soils and Clay Minerals* (pp. 83–98). Springer Netherlands. https://doi.org/10.1007/978-94-009-4007-9_5

Brouwer, P. (2010). *Theory of XRF: Getting acquainted with the principles* (3rd ed.). PANalytical B.V.

Buurman, P., van Lagen, B., & Velthorst, E. J. (1996). Section A - soil analysis. In *Manual for Soil and Water Analysis* (pp. 1–116). Backhuys Publishers.

Climate Data. (2024). *Klima Corleone: Temperatur, Klimatabelle & Klimadiagramm für Corleone + Wetter*. https://de.climate-data.org/europa/italien/sizilien/corleone-13871/

Clough, A., & Skjemstad, J. O. (2000). Physical and chemical protection of soil organic carbon in three agricultural soils with different contents of calcium carbonate. *Australian Journal of Soil Research*, *38*(5), 1005–1016. Scopus. https://doi.org/10.1071/SR99102

Cornell, R. M., & Schwertmann, U. (2003). *The Iron Oxides: Structure, Properties, Reactions, Occurrences and Uses* (2nd ed.). Wiley.

Cortijos-López, M., Sánchez-Navarrete, P., de la Parra-Muñoz, I., Lasanta, T., & Nadal-Romero, E. (2024). A strategy to enhance soil quality and soil organic carbon stock in abandoned lands: Pasture regeneration through shrub clearing. *Land Degradation & Development*, *35*(10), 3392–3406. https://doi.org/10.1002/ldr.5139

Edwards, T. (2024). *What is soil organic carbon?* https://www.agric.wa.gov.au/measuring-and-assessing-soils/what-soil-organic-carbon

Egli, M., Alioth, L., Mirabella, A., Raimondi, S., Nater, M., & Verel, R. (2007). Effect of Climate and Vegetation on Soil Organic Carbon, Humus Fractions, Allophanes, Imogolite, Kaolinite, and Oxyhydroxides in Volcanic Soils of Etna (Sicily). *Soil Science*, *172*(9), 673. https://doi.org/10.1097/ss.0b013e31809eda23

Egli, M., Bösiger, M., Lamorski, K., Sławiński, C., Plötze, M., Wiesenberg, G. L. B., Tikhomirov, D., Musso, A., Hsu, S.-Y., & Raimondi, S. (2021). Pedogenesis and carbon sequestration in transformed agricultural soils of Sicily. *Geoderma*, *402*, 115355. https://doi.org/10.1016/j.geoderma.2021.115355

Egli, M., Zhang, M.-G., Plötze, M., Tema, E., Mohammadi, M., Wang, Q.-B., & Raimondi, S. (2024). Soil development trajectories, chemical weathering and pedogenic mineral (trans)formation on glauconitic calcarenites in a Mediterranean area. *CATENA*, *243*, 108177. https://doi.org/10.1016/j.catena.2024.108177

FAO. (2025, January 8). *Global Soil Organic Carbon Map*. Global Soil Information System. https://data.apps.fao.org/glosis/?share=f-6756da2a-5c1d-4ac9-9b94-297d1f105e83&lang=en

Fernandes, M. R., Aguiar, F. C., Martins, M. J., Rico, N., Ferreira, M. T., & Correia, A. C. (2020). Carbon Stock Estimations in a Mediterranean Riparian Forest: A Case Study Combining Field Data and UAV Imagery. *Forests*, *11*(4), Article 4. https://doi.org/10.3390/f11040376

Fornara, D. A., Steinbeiss, S., McNAMARA, N. P., Gleixner, G., Oakley, S., Poulton, P. R., Macdonald, A. J., & Bardgett, R. D. (2011). Increases in soil organic carbon sequestration can reduce the global warming potential of long-term liming to permanent grassland. *Global Change Biology*, *17*(5), 1925–1934. https://doi.org/10.1111/j.1365-2486.2010.02328.x

Funes, I., Savé, R., Rovira, P., Molowny-Horas, R., Alcañiz, J. M., Ascaso, E., Herms, I., Herrero, C., Boixadera, J., & Vayreda, J. (2019). Agricultural soil organic carbon stocks in the north-eastern Iberian Peninsula: Drivers and spatial variability. *Science of The Total Environment*, *668*, 283–294. https://doi.org/10.1016/j.scitotenv.2019.02.317

Georgiou, K., Jackson, R. B., Vindušková, O., Abramoff, R. Z., Ahlström, A., Feng, W., Harden, J. W., Pellegrini, A. F. A., Polley, H. W., Soong, J. L., Riley, W. J., & Torn, M. S. (2022). Global stocks and capacity of mineral-associated soil organic carbon. *Nature Communications*, *13*(1), 3797. https://doi.org/10.1038/s41467-022-31540-9

Gerke, H. H., Rieckh, H., & Sommer, M. (2016). Interactions between crop, water, and dissolved organic and inorganic carbon in a hummocky landscape with erosion-affected pedogenesis. *Soil and Tillage Research*, *156*, 230–244. https://doi.org/10.1016/j.still.2015.09.003

Gerke, J. (2022). The Central Role of Soil Organic Matter in Soil Fertility and Carbon Storage. *Soil Systems*, *6*(2), Article 2. https://doi.org/10.3390/soilsystems6020033

Giannitrapani, E. (1998). Public archaeology and prehistory in Sicily. *Antiquity*, *72*(278), 739–743. https://doi.org/10.1017/S0003598X00087305

Hassink, J. (1997). The capacity of soils to preserve organic C and N by their association with clay and silt particles. *Plant and Soil*, *191*(1), 77–87. https://doi.org/10.1023/A:1004213929699

Herzog, C., Hartmann, M., Frey, B., Stierli, B., Rumpel, C., Buchmann, N., & Brunner, I. (2019). Microbial succession on decomposing root litter in a drought-prone Scots pine forest. *The ISME Journal*, *13*(9), 2346–2362. https://doi.org/10.1038/s41396-019-0436-6

Hesse, R., & Schacht, U. (2011). Chapter 9—Early Diagenesis of Deep-Sea Sediments. In H. Hüneke & T. Mulder (Eds.), *Developments in Sedimentology* (Vol. 63, pp. 557–713). Elsevier. https://doi.org/10.1016/B978-0-444-53000-4.00009-3

Huang, Y., Song, X., Wang, Y.-P., Canadell, J. G., Luo, Y., Ciais, P., Chen, A., Hong, S., Wang, Y., Tao, F., Li, W., Xu, Y., Mirzaeitalarposhti, R., Elbasiouny, H., Savin, I., Shchepashchenko, D., Rossel, R. A. V., Goll, D. S., Chang, J., … Zhang, G.-L. (2024). Size, distribution, and vulnerability of the global soil inorganic carbon. *Science*, *384*(6692), 233–239. https://doi.org/10.1126/science.adi7918

Instituto Superiore per la Protezione e la Ricerca Ambientale (ISPRA). (2024). *Carta Geologica d'Italia 1:50.000*. https://www.isprambiente.gov.it/Media/carg/sicilia.html

IUSS Working Group WRB. (2022). *World Reference Base for Soil Resources. International soil classification system for naming soils and creating legends for soil maps* (4th ed.). International Union of Soil Sciences.

Jiménez-Ballesta, R., Bravo, S., Pérez-de-los-Reyes, C., Amorós, J. A., & García-Navarro, F. J. (2023). Carbonate morphological features of vineyard soils in a semiarid Mediterranean environment. *European Journal of Soil Science*, *74*(6), e13435. https://doi.org/10.1111/ejss.13435

Jobbágy, E. G., & Jackson, R. B. (2000). The Vertical Distribution of Soil Organic Carbon and Its Relation to Climate and Vegetation. *Ecological Applications*, *10*(2), 423–436. https://doi.org/10.1890/1051-0761(2000)010[0423:TVDOSO]2.0.CO;2

Johansson, M., Braakenburg, N. E., Stow, D. A. V., & Faugères, J.-C. (1998). Deep-water massive sands: Facies, processes and channel geometry in the Numidian Flysch, Sicily. *Sedimentary Geology*, *115*(1), 233–265. https://doi.org/10.1016/S0037-0738(97)00095-X

Kaiser, K., & Zech, W. (1996). Defects in estimation of aluminum in humus complexes of pdzolic soils by pyrophosphate extraction. *Soil Science*, *161*(7), 452.

Kohn, M. J. (2010). Carbon isotope compositions of terrestrial C3 plants as indicators of (paleo)ecology and (paleo)climate. *Proceedings of the National Academy of Sciences*, *107*(46), 19691–19695. https://doi.org/10.1073/pnas.1004933107

Laban, P., Metternicht, G., & Davies, J. (2018). *Soil biodiversity and soil organic carbon: Keeping drylands alive* (1st ed.). IUCN, International Union for Conservation of Nature. https://doi.org/10.2305/IUCN.CH.2018.03.en

Lal, R. (2004). Soil Carbon Sequestration Impacts on Global Climate Change and Food Security. *Science*, *304*(5677), 1623–1627. https://doi.org/10.1126/science.1097396

Laudicina, V. A., Novara, A., Barbera, V., Egli, M., & Badalucco, L. (2015). Long-Term Tillage and Cropping System Effects on Chemical and Biochemical Characteristics of Soil Organic Matter in a Mediterranean Semiarid Environment. *Land Degradation & Development*, *26*(1), 45–53. https://doi.org/10.1002/ldr.2293

Lavallee, J. M., Soong, J. L., & Cotrufo, M. F. (2020). Conceptualizing soil organic matter into particulate and mineral-associated forms to address global change in the 21st century. *Global Change Biology*, *26*(1), 261–273. https://doi.org/10.1111/gcb.14859

Li, C., Wang, H., Zhao, L., & Shen, H. (2024). Effect of long-term land use change on soil organic carbon fractions and functional groups. *Arid Land Research and Management*, *38*(2), 182–200. https://doi.org/10.1080/15324982.2023.2284882

Lin, H. (2011). Three Principles of Soil Change and Pedogenesis in Time and Space. *Soil Science Society of America*, *75*(6), 2049–2070. https://doi.org/10.2136/sssaj2011.0130

Lozano-García, B., Muñoz-Rojas, M., & Parras-Alcántara, L. (2017). Climate and land use changes effects on soil organic carbon stocks in a Mediterranean semi-natural area. *Science of The Total Environment*, *579*, 1249–1259. https://doi.org/10.1016/j.scitotenv.2016.11.111

Mainka, M., Summerauer, L., Wasner, D., Garland, G., Griepentrog, M., Berhe, A. A., & Doetterl, S. (2022). Soil geochemistry as a driver of soil organic matter composition: Insights from a soil chronosequence. *Biogeosciences*, *19*(6), 1675–1689. https://doi.org/10.5194/bg-19-1675-2022

Marino, P., Bazan, G., & Luczo, S. (2017). *Protecting Biodiversity on Private Property: An Experience in Corleone (Sicily)*. IT.

Martí-Roura, M., Hagedorn, F., Rovira, P., & Romanyà, J. (2019). Effect of land use and carbonates on organic matter stabilization and microbial communities in Mediterranean soils. *Geoderma*, *351*, 103–115. https://doi.org/10.1016/j.geoderma.2019.05.021

Mastrolonardo, G., Certini, G., Krebs, R., Forte, C., & Egli, M. (2013). Effects of fire on soil organic matter quality along an altitudinal sequence on Mt. Etna, Sicily. *CATENA*, *110*, 133–145. https://doi.org/10.1016/j.catena.2013.05.017

Michelangeli, F., Di Rita, F., Lirer, F., Lubritto, C., Bellucci, L. G., Cascella, A., Bonomo, S., Margaritelli, G., & Magri, D. (2022). Vegetation history of SE Sicily from feudal land management to post-war agricultural industrialization. *Review of Palaeobotany and Palynology*, *296*, 104547. https://doi.org/10.1016/j.revpalbo.2021.104547

Naorem, A., Jayaraman, S., Dalal, R. C., Patra, A., Rao, C. S., & Lal, R. (2022). Soil Inorganic Carbon as a Potential Sink in Carbon Storage in Dryland Soils—A Review. *Agriculture*, *12*(8), Article 8. https://doi.org/10.3390/agriculture12081256

Nesbitt, H. W., & Young, G. M. (1982). Early Proterozoic climates and plate motions inferred from major element chemistry of lutites. *Nature*, *299*(5885), 715–717. https://doi.org/10.1038/299715a0

Novara, A., Gristina, L., Sala, G., Galati, A., Crescimanno, M., Cerdà, A., Badalamenti, E., & La Mantia, T. (2017). Agricultural land abandonment in Mediterranean environment provides ecosystem services via soil carbon sequestration. *Science of The Total Environment*, *576*, 420–429. https://doi.org/10.1016/j.scitotenv.2016.10.123

Orme, G. R. (1984). Calcarenite. In M. Schwartz (Ed.), *Beaches and Coastal Geology* (pp. 186–186). Springer US. https://doi.org/10.1007/0-387-30843-1_86

Pansu, M., & Gautheyrou, J. (Eds.). (2006a). pH Measurement. In *Handbook of Soil Analysis: Mineralogical, Organic and Inorganic Methods* (pp. 551–579). Springer. https://doi.org/10.1007/978-3-540-31211-6_15

Pansu, M., & Gautheyrou, J. (Eds.). (2006b). Water Content and Loss on Ignition. In *Handbook of Soil Analysis: Mineralogical, Organic and Inorganic Methods* (pp. 3–13). Springer. https://doi.org/10.1007/978-3-540-31211-6_1

Parker, A. (1970). An Index of Weathering for Silicate Rocks. *Geological Magazine*, *107*(6), 501–504. https://doi.org/10.1017/S0016756800058581

Phillips, J. D. (2017). Soil Complexity and Pedogenesis. *Soil Science*, *182*(4), 117. https://doi.org/10.1097/SS.0000000000000204

Quijano, L., Van Oost, K., Nadeu, E., Gaspar, L., & Navas, A. (2017). Modelling the Effect of Land Management Changes on Soil Organic Carbon Stocks in a Mediterranean Cultivated Field. *Land Degradation & Development*, *28*(2), 515–523. https://doi.org/10.1002/ldr.2637

Raimondi, S., & Pirrone, A. (2020). Land Cadastre in Italy for Sustainable Development: Application to Two Parcels of Land in a Geopark in the Process of Being Defined in Corleone. *Open Journal of Humanities*, *5*, 119–161. https://doi.org/10.17605/osf.io/extcb

Regione Siciliana. (2024). *Riserva Naturale Bosco della Ficuzza, Rocca Busambra, Gorgo del Drago, Bosco del Cappelliere*. Osservatorio Regionale Biodiversità Siciliana. https://orbs.regione.sicilia.it/aree-protette/riserve-naturali-siciliane/172-riserva-naturale-bosco-della-ficuzza-rocca-busambra-gorgo-del-drago-bosco-del-cappelliere.html

Rey, A., Petsikos, C., Jarvis, P. G., & Grace, J. (2005). Effect of temperature and moisture on rates of carbon mineralization in a Mediterranean oak forest soil under controlled and field conditions. *European Journal of Soil Science*, *56*(5), 589–599. https://doi.org/10.1111/j.1365-2389.2004.00699.x

Rodeghiero, M., Rubio, A., Díaz-Pinés, E., Romanyà, J., Marañón-Jiménez, S., Levy, G. J., Fernandez-Getino, A. P., Sebastià, M. T., Karyotis, T., Chiti, T., Sirca, C., Martins, A., Madeira, M., Zhiyanski, M., Gristina, L., & La Mantia, T. (2011). Soil Carbon in Mediterranean Ecosystems and Related Management Problems. In *Soil Carbon in Sensitive European Ecosystems* (pp. 175–218). John Wiley & Sons, Ltd. https://doi.org/10.1002/9781119970255.ch8

Rovira, P., Casals, P., Romanyà, J., Bottner, P., Coûteaux, M.-M., & Ramon Vallejo, V. (1998). Recovery of fresh debris of different sizes in density fractions of two contrasting soils. *European Journal of Soil Biology*, *34*(1), 31–37. https://doi.org/10.1016/S1164-5563(99)80004-1

Scharlemann, J. P., Tanner, E. V., Hiederer, R., & Kapos, V. (2014). Global soil carbon: Understanding and managing the largest terrestrial carbon pool. *Carbon Management*, *5*(1), 81–91. https://doi.org/10.4155/cmt.13.77

Singh, M., Sarkar, B., Sarkar, S., Churchman, J., Bolan, N., Mandal, S., Menon, M., Purakayastha, T. J., & Beerling, D. J. (2018). Chapter Two—Stabilization of Soil Organic Carbon as Influenced by Clay Mineralogy. In D. L. Sparks (Ed.), *Advances in Agronomy* (Vol. 148, pp. 33–84). Academic Press. https://doi.org/10.1016/bs.agron.2017.11.001

Six, J., Bossuyt, H., Degryze, S., & Denef, K. (2004). A history of research on the link between (micro)aggregates, soil biota, and soil organic matter dynamics. *Soil and Tillage Research*, *79*(1), 7–31. https://doi.org/10.1016/j.still.2004.03.008

Six, J., Callewaert, P., Lenders, S., De Gryze, S., Morris, S. J., Gregorich, E. G., Paul, E. A., & Paustian, K. (2002). Measuring and Understanding Carbon Storage in Afforested Soils by Physical Fractionation. *Soil Science Society of America Journal*, *66*(6), 1981–1987. https://doi.org/10.2136/sssaj2002.1981

Six, J., Carpentier, A., Van Kessel, C., Merckx, R., Harris, D., Horwath, W. R., & Lüscher, A. (2001). Impact of elevated CO2 on soil organic matter dynamics as related to changes in aggregate turnover and residue quality. *Plant and Soil*, *234*(1), 27–36. Scopus. https://doi.org/10.1023/A:1010504611456

Six, J., Conant, R. T., Paul, E. A., & Paustian, K. (2002). Stabilization mechanisms of soil organic matter: Implications for C-saturation of soils. *Plant and Soil*, *241*(2), 155–176. https://doi.org/10.1023/A:1016125726789

Smith, P., Cotrufo, M. F., Rumpel, C., Paustian, K., Kuikman, P. J., Elliott, J. A., McDowell, R., Griffiths, R. I., Asakawa, S., Bustamante, M., House, J. I., Sobocká, J., Harper, R., Pan, G., West, P. C., Gerber, J. S., Clark, J. M., Adhya, T., Scholes, R. J., & Scholes, M. C. (2015). Biogeochemical cycles and biodiversity as key drivers of ecosystem services provided by soils. *SOIL*, *1*(2), 665–685. https://doi.org/10.5194/soil-1-665-2015

Spatafora, F. (1996, September). *La vecchia di Corleone*. Archeologia Viva. https://www.archeologiaviva.it/5387/la-vecchia-di-corleone/

Sun, S. S., & McDonough, W. F. (1989). Chemical and isotopic systematics of oceanic basalts: Implications for mantle composition and processes. In *Magmatism in the ocean basins* (42nd ed., pp. 313–345). https://10.1144/GSL.SP.1989.042.01.19

Tribovillard, N., Bout-Roumazeilles, V., Abraham, R., Ventalon, S., Delattre, M., & Baudin, F. (2023). The contrasting origins of glauconite in the shallow marine environment highlight this mineral as a marker of paleoenvironmental conditions. *Comptes Rendus. Géoscience*, *355*(S2), 213–228. https://doi.org/10.5802/crgeos.170

Venturella, G. (2004). Climatic and pedological features of Sicily. *Bocconea*, *17*, 47–53.

Viret, F., & Grand, S. (2019). Combined Size and Density Fractionation of Soils for Investigations of Organo-Mineral Interactions. *Journal of Visualized Experiments: JoVE*, *144*. https://doi.org/10.3791/58927

Weil, R. R., Brady, N. C., & Weil, R. R. (with Brady, N. C.). (2017). *The nature and properties of soils* (Fifteenth edition, global edition). Pearson.

Wiesmeier, M., Urbanski, L., Hobley, E., Lang, B., Von Lützow, M., Marin-Spiotta, E., Van Wesemael, B., Rabot, E., Ließ, M., Garcia-Franco, N., Wollschläger, U., Vogel, H.-J., & Kögel-Knabner, I. (2019). Soil organic carbon storage as a key function of soils—A review of drivers and indicators at various scales. *Geoderma*, *333*, 149–162. https://doi.org/10.1016/j.geoderma.2018.07.026

Willaarts, B. A., Oyonarte, C., Muñoz-Rojas, M., Ibáñez, J. J., & Aguilera, P. A. (2016). Environmental Factors Controlling Soil Organic Carbon Stocks in Two Contrasting Mediterranean Climatic Areas of Southern Spain. *Land Degradation & Development*, *27*(3), 603–611. https://doi.org/10.1002/ldr.2417

Zhao, Z., Zhao, Z., Fu, B., Wang, J., & Tang, W. (2021). Characteristics of soil organic carbon fractions under different land use patterns in a tropical area. *Journal of Soils and Sediments*, *21*(2), 689–697. https://doi.org/10.1007/s11368-020-02809-7

Zhou, W., Han, G., Liu, M., & Li, X. (2019). Effects of soil pH and texture on soil carbon and nitrogen in soil profiles under different land uses in Mun River Basin, Northeast Thailand. *PeerJ*, *7*, e7880. https://doi.org/10.7717/peerj.7880

Zollinger, B., Alewell, C., Kneisel, C., Meusburger, K., Gärtner, H., Brandová, D., Ivy-Ochs, S., Schmidt, M. W. I., & Egli, M. (2013). Effect of permafrost on the formation of soil organic carbon pools and their physical–chemical properties in the Eastern Swiss Alps. *CATENA*, *110*, 70–85. https://doi.org/10.1016/j.catena.2013.06.010

7 Declaration of the usage of AI

I have composed the contents of this work independently, but with the use of ChatGPT (https://chatopenai.com, 2025) for enhancing language and check for spelling errors.

The prompt used was “Proofread this paragraph for me and if necessary, help improve language”.

Personal declaration:

I hereby declare that the submitted thesis is the result of my own, independent work. All external sources are explicitly acknowledged in the thesis

Zürich, 25.04.2025

Annette den Boer